

**PURDUE UNIVERSITY**  
**GRADUATE SCHOOL**  
**Thesis/Dissertation Acceptance**

This is to certify that the thesis/dissertation prepared

By AISHWARYA RAMAMURTHY

Entitled  
INVESTIGATING THE EARLY EVENTS IN PROTEASOME ASSEMBLY

For the degree of Master of Science

Is approved by the final examining committee:

Dr. ANDREW KUSMIERCZYK

Dr. SIMON ATKINSON

Dr. STEPHEN RANDALL

To the best of my knowledge and as understood by the student in the *Thesis/Dissertation Agreement, Publication Delay, and Certification/Disclaimer (Graduate School Form 32)*, this thesis/dissertation adheres to the provisions of Purdue University's "Policy on Integrity in Research" and the use of copyrighted material.

Dr. Andrew Kusmierczyk

Approved by Major Professor(s): \_\_\_\_\_

Approved by: Dr. Simon Atkinson

06/30/2014

Head of the Department Graduate Program

Date

INVESTIGATING THE EARLY EVENTS IN PROTEASOME ASSEMBLY

A Thesis

Submitted to the Faculty

of

Purdue University

by

Aishwarya Ramamurthy

In Partial Fulfillment of the

Requirements for the Degree

of

Master of Science

August 2014

Purdue University

Indianapolis, Indiana

*To my parents*

## ACKNOWLEDGEMENTS

I would like to thank Dr. Andrew Kusmierczyk for his guidance, incessant support and encouragement throughout the course of this project. I am extremely grateful for the opportunity to work in his lab. I would like to thank my committee members, Dr. Stephen Randall and Dr. Simon Atkinson for their time, advice and support. I would also like to thank my fellow lab members for making my work period constructive and my learning experience most enjoyable.

## TABLE OF CONTENTS

	Page
LIST OF TABLES .....	vi
LIST OF FIGURES .....	vii
LIST OF ABBREVIATIONS.....	ix
ABSTRACT.....	xi
CHAPTER 1. INTRODUCTION .....	1
1.1 Protein Degradation by the Ubiquitin Proteasome System.....	1
1.2 Structure of the 26S Proteasome.....	2
1.2.1 20S Proteasomes in Archaea and Bacteria .....	3
1.3 Assembly of the 20S Proteasome .....	4
1.3.1 Chaperone Proteins in Assembly .....	4
1.3.2 Self-assembly of Proteasomal Subunits.....	6
1.3.3 Self-assembly of $\alpha$ subunits into Higher Order Structures .....	6
1.4 Objectives .....	8
CHAPTER 2. MATERIALS AND METHODS .....	10
2.1 Cloning and Transformation .....	10
2.2 Protein Induction .....	10
2.3 Bacterial Lysis and Protein Purification .....	11
2.4 Protein Expression Profiling .....	12
2.5 Native PAGE Analysis .....	12
2.6 Detection of Cross-linked Bands .....	12
2.7 Reversibility of Cross-linking.....	14
CHAPTER 3. RESULTS AND DISCUSSION.....	15
3.1 Higher Order Complexes of <i>S. cerevisiae</i> $\alpha$ subunits .....	15

	Page
3.2 Formation of $\alpha$ - $\alpha$ Double Rings in Archaea .....	17
3.3 Crosslinking Analysis of AKB80 ( $\alpha 5\alpha 6\alpha 7\alpha 1$ -His) and its Mutants.....	22
3.3.1 Resolving the Noise Caused by Native Cysteines .....	24
3.4 Cross-linking Analysis of AKB80 ( $\alpha 5\alpha 6\alpha 7\alpha 1$ -his) in Purified Eluates .....	25
3.4.1 Analysis with Cross-linkable Cysteine in $\alpha 1$ .....	26
3.4.2 Analysis with Cross-linkable cysteine in $\alpha 7$ .....	27
3.4.3 Analysis with Cross-linkable cysteine in $\alpha 7$ and $\alpha 1$ .....	28
3.5 Cross-linking analysis of AKB80 ( $\alpha 5\alpha 6\alpha 7\alpha 1$ -his) in Native Complexes .....	29
3.5.1 Analysis with Cross-linkable Cysteine in $\alpha 1$ .....	29
3.5.2 Analysis with Cross-linkable Cysteine in $\alpha 7$ .....	30
3.5.3 Analysis with Cross-linkable Cysteine in $\alpha 7$ and $\alpha 1$ .....	31
3.6 Identifying $\alpha 1$ - $\alpha 1$ Crosslinks in Higher Order Complexes other than of AKB80 ( $\alpha 5\alpha 6\alpha 7\alpha 1$ -his) .....	31
CHAPTER 4. CONCLUSIONS AND FUTURE DIRECTIONS .....	34
REFERENCES .....	39
TABLES .....	43
FIGURES .....	45

## LIST OF TABLES

Table	Page
Table 1. Proteasome and protein conjugation system across the domains of life.....	43
Table 2. Plasmids used in this study .....	44

## LIST OF FIGURES

Figure	Page
Figure 1. Structure of the proteasome .....	45
Figure 2. Model for assembly of 20S CP in yeast .....	46
Figure 3. Archaeal $\alpha$ subunits form double rings .....	47
Figure 4. $\alpha$ subunits of <i>T. acidophilum</i> .....	48
Figure 5. Subunit contacts between an $\alpha$ (red) and $\beta$ (blue) subunit, viewed from inside the 20S cavity .....	49
Figure 6. Efficient double ring formation in the presence of a cross-linkable cysteine in $\alpha$ subunit .....	50
Figure 7. Presence of cross-linked $\alpha$ - $\alpha$ dimer bands in archaeal double rings .....	51
Figure 8. Efficient double ring formation depends on the position of the introduced cross-linkable cysteine .....	52
Figure 9. ClustalW alignment of $\alpha$ subunits from <i>T. acidophilum</i> , <i>M. maripaludis</i> , and $\alpha 5$ , $\alpha 6$ , $\alpha 7$ , $\alpha 1$ from <i>S. cerevisiae</i> .....	53
Figure 10. Expression profiling of AKB80 mutants. AKB80, AKB752, AKB753 and AKB754 were expressed in <i>E. coli</i> .....	54
Figure 11. Detection of cross-linked bands in AKB80 mutants with introduced cross-linkable cysteine .....	55
Figure 12. Detection of cross-linked bands in AKB80 mutants with cross-linkable cysteine but no internal cysteines .....	56
Figure 13. Crosslinking analysis of AKB80 and its mutant with cross-linkable cysteine in $\alpha 1$ .....	57
Figure 14. Reduction of cross-linked bands from AKB788 .....	58

Figure	Page
Figure 15. Crosslinking analysis of an AKB80 mutant with cross-linkable cysteine in $\alpha 7$ .....	59
Figure 16. Crosslinking analysis of an AKB80 mutant with cross-linkable cysteine in $\alpha 7$ and $\alpha 1$ .....	60
Figure 17. Reduction of cross-linked bands from AKB789 .....	61
Figure 18. High molecular weight complexes in AKB80 and AKB788 .....	62
Figure 19. Crosslinking analysis of high molecular weight complexes (HMWCs) formed by AKB788 .....	63
Figure 20. High molecular weight complexes in AKB785 and AKB786 .....	64
Figure 21. Crosslinking analysis of high molecular weight complexes (HMWCs) formed by AKB785 and AKB786.....	65
Figure 22. High molecular weight complexes in AKB796 and AKB789 .....	66
Figure 23. Crosslinking analysis of high molecular weight complexes (HMWCs) formed by AKB796 and AKB789.....	67
Figure 24. High molecular weight complexes formed when $\alpha 5$ , $\alpha 6$ , $\alpha 7$ and $\alpha 1$ are co-expressed in different combinations .....	68
Figure 25. Crosslinking analysis of high molecular weight complexes (HMWCs) formed when $\alpha 7$ and $\alpha 1$ are co-expressed.....	69
Figure 26. Crosslinking analysis of high molecular weight complexes (HMWCs) formed when $\alpha 6$ , $\alpha 7$ and $\alpha 1$ are co-expressed .....	70

## LIST OF ABBREVIATIONS

°C	Degrees Celsius
19S RP	19S Regulatory Particle
20S CP	20S Core Particle
Arc	AAA+ ATPase forming a Ring shaped Complex
DTT	Dithiothreitol
EM	Electron Microscopy
HbYX	Hydrophobic-tyrosine-any amino acid tripeptide
HMWC	High Molecular Weight Complex
IMAC	Immobilized Metal Ion Chromatography
IPTG	Isopropyl $\beta$ -D-1-thiogalactopyranoside
kDa	Kilodalton
LB	Lysogeny Broth
$\mu$ L	Microliter
$\mu$ M	Micromolar

mL	Milliliter
mM	Millimolar
Mpa	Mycobacterial proteasome ATPase
MS	Mass Spectrometry
MW	Molecular Weight
NTA	Nitrilotriacetic Acid
pI	Isoelectric point
PAGE	Polyacrylamide Gel Electrophoresis
PAN	Proteasome Activating Nucleotidase
RPM	Rotations Per Minute
SDS	Sodium Dodecyl Sulfate
UPS	Ubiquitin Protease System

## ABSTRACT

Ramamurthy, Aishwarya. M.S., Purdue University, August 2014. Investigating the early events in proteasome assembly. Major Professor: Andrew Kusmierczyk.

Proteasome assembly is a rapid and highly sequential process that occurs through a series of intermediates. While the quest to understand the exact process of assembly is ongoing, there remains an incomplete understanding of what happens early on during the process, prior to the involvement of the  $\beta$  subunits. A significant feature of proteasome assembly is the property of proteasomal subunits to self-assemble. While archaeal  $\alpha$  and  $\beta$  subunits from *Thermoplasma acidophilum* can assemble into entire 20S units in vitro, certain  $\alpha$  subunits from divergent species have a property to self-assemble into single and double heptameric rings. In this study, we have shown that recombinant  $\alpha$  subunits from *Methanococcus maripaludis* also have a tendency to self-assemble into higher order structures when expressed in *E. coli*. Using a novel cross-linking strategy, we were able to establish that these higher order structures were double  $\alpha$  rings that are structurally similar to a half-proteasome (i.e. an  $\alpha$ - $\beta$  ring pair). Our experiments on *M. maripaludis*  $\alpha$  subunits represent the first biochemical evidence for the orientation of rings in an  $\alpha$  ring dimer. We also investigated self-assembly of  $\alpha$  subunits in *S. cerevisiae* and attempted to

characterize a highly stable and unique high molecular weight complex (HMWC) that is formed upon co-expression of  $\alpha 5$ ,  $\alpha 6$ ,  $\alpha 7$  and  $\alpha 1$  in *E. coli*. Using our cross-linking strategy, we were able to show that this complex is a double  $\alpha$  ring in which, at the least, one  $\alpha 1$  subunit is positioned across itself. We were also able to detect  $\alpha 1$ - $\alpha 1$  crosslinks in high molecular weight complexes that are formed when  $\alpha 7$  and  $\alpha 1$  are co-expressed, and when  $\alpha 6$ ,  $\alpha 7$  and  $\alpha 1$  are co-expressed in *E. coli*. The fact that we able to observe  $\alpha 1$ - $\alpha 1$  crosslinks in higher order structures that form whenever  $\alpha 7$  and  $\alpha 1$  were present suggests that  $\alpha 1$ - $\alpha 1$  crosslinks might be able to serve as potential trackers to detect HMWCs in vivo. This would be an important step in determining if these HMWCs represent bona fide assembly intermediates, or dead-end complexes whose formation must be prevented in order to ensure efficient proteasome assembly.

## CHAPTER 1. INTRODUCTION

### 1.1 Protein degradation by the Ubiquitin Proteasome System

Protein degradation is an important aspect of protein quality control and cellular homeostasis. It occurs in many ways across all living organisms. In eukaryotes, of high significance is the ubiquitin proteasome system (UPS) which selectively degrades misfolded, damaged and transient regulatory proteins via multicatalytic barrel-like protease complexes called proteasomes (Wilk and Orłowski, 1983). Selectivity of proteins degraded by the UPS is conferred upon by the presence of ubiquitin molecules on the target protein. This process begins with the covalent attachment of a single ubiquitin molecule to the target protein, followed by the incorporation of multiple molecules of ubiquitin to form a polyubiquitin tag. This tag is recognized by the proteasome which then proceeds to degrade the substrate protein. The ubiquitin proteasome system is highly relevant in maintaining intracellular equilibrium, and defects in this system have been implicated in viral infections, neurodegenerative diseases and in cancer (Fang and Weissman, 2004).

## 1.2 Structure of the 26S Proteasome

The 26S proteasome in eukaryotes is made up of a 20S core particle (CP) and a 19S regulatory particle (RP) (Figure 1a). The 20S CP has a cylindrical structure composed of twenty eight subunits arranged in the form of four heptameric rings, one above the other (Groll et al., 1997). The outer two rings are made of seven different  $\alpha$  subunits ( $\alpha 1$ -  $\alpha 7$ ; Figure 1b) while the inner two rings are made of seven different  $\beta$  subunits ( $\beta 1$ -7). The proteolytic core of the proteasome is formed by the 20S CP wherein proteolytic activity resides in the catalytic sites of  $\beta 1$  (caspase like specificity),  $\beta 2$  (trypsin like specificity), and  $\beta 5$  (chymotrypsin like specificity). These three subunits are synthesized with propeptides that conceal the active sites on the subunits. The propeptides are autocatalytically cleaved to give rise to a functionally active proteasome (Groll et al., 1997; Chen and Hochstrasser, 1995).

The 19S Regulatory Particle (19S RP) is made of nineteen subunits and caps the 20S CP on either or both sides. It is conventionally described as having two distinct regions – a base region and a lid. The base associates with the  $\alpha$  ring, and is made of six related AAA-ATPase subunits (Rpt1-6) that assemble into a hexameric ring, and four non ATPase subunits (Rpn 1, 2, 10 and 13). The lid is made of nine other non-ATPase subunits (Rpn 3, 5-9, 11, 12) and was formerly thought to be positioned above the basal ring (Glickman et al., 1998). Recent studies reveal that the lid is positioned more proximal and lateral to the top of the 20S CP than previously thought (Figure 1c) (Beck et al., 2012; Lander et al., 2012).

The 19S RP binds to the  $\alpha$  ring of CP through a HbYX (hydrophobic-tyrosine-any amino acid tripeptide) motif present in the C-terminus of Rpt subunits (Gillette et al., 2008). Binding of the 19S to the 20S CP, which is normally in a closed state, brings about conformational changes on the latter that in turn lead to opening of the CP for substrate entry and degradation. The 19S RP is also functional in recognition, deubiquitination and unfolding of the protein substrate for degradation (Finley, 2009).

### 1.2.1 20S Proteasomes in Archaea and Bacteria

20S proteasomes are also found in archaea and in the actinomycete lineage of bacteria. Similar to those found in the eukaryotes, these 20S proteasomes have two inner  $\beta$  subunit heptameric rings and two outer  $\alpha$  subunit heptameric rings. However, they are less complex than the eukaryotic 20S CP in that there are just one or two types of  $\alpha$  subunits and one or two types of  $\beta$  subunits constituting the CP (Tamura et al., 1995, Zwickl et al., 1999). The proteolytic activity of these proteasomes too, includes chymotryptic, tryptic and/or peptidylglutamyl peptide hydrolyzing activities and resides in the catalytic site of each  $\beta$  subunit (Maupin-Furlow, 2011).

While 19S RPs cap the eukaryotic 20S CP, functionally similar structures called Proteasome-Activating Nucleotidase (PAN), which are ATPase complexes, cap the archaeal 20S proteasomes and effectuate increased proteasome activity (Zwickl et al., 1999). Like the 19S RP, PAN has a conserved HbYX motif at the C-terminus through which it associates with the 20S CP and brings about opening of the latter for substrate entry (Smith et al., 2007). It is interesting to note that PAN also has the ability to refold denatured proteins and independently function as a molecular chaperone (Benaroudj and

Goldberg, 2000). In actinomycetes, the AAA-ATPase regulators of 20S proteasomes are referred to as AAA+ ATPase forming a Ring-shaped Complex (Arc); Arc is also known as Mycobacterial proteasome ATPase (Mpa) in *Mycobacterium tuberculosis* (Maupin-Furlow, 2011) (Table 1).

### 1.3 Assembly of the 20S Proteasome

Though much is known about the structure and function of the proteasome, considerably less is known about how this large molecular machine is assembled in the first place. Current understanding of the eukaryotic 20S proteasome assembly depicts  $\alpha$  ring formation as the first step, and individual  $\beta$  subunits are incorporated atop the  $\alpha$  ring template (Figure 2). In *S. cerevisiae*, a complete  $\alpha$  ring with  $\beta 2$ ,  $\beta 3$  and  $\beta 4$  structure was identified as the earliest stable assembly intermediate, and is referred to as the 15S complex (Li et al., 2007). Using a mammalian cell line model, the order of  $\beta$  subunit incorporation was deduced to be  $\beta 2$ ,  $\beta 3$ ,  $\beta 4$ ,  $\beta 5$ ,  $\beta 6$ ,  $\beta 1$  and  $\beta 7$  (Hirano et al., 2008). Fully formed  $\alpha\beta$  rings (i.e. half-proteasomes) dimerize to form the symmetric immature CP that undergoes autocatalytic processing of  $\beta$  propeptides to form a mature and functional CP. Archaeal proteasomes use a similar  $\alpha$ -ring-first pathway to reach the half-proteasome stage, while actinomycete  $\alpha$  and  $\beta$  subunits form heterodimers first and these heterodimers then assemble into half-proteasomes directly (Maupin-Furlow, 2011).

#### 1.3.1 Chaperone Proteins in Assembly

Various dedicated chaperones are known to guide proteasome assembly intermediates through their assembly pathway (Figure 2). For example, Ump1 is a short-

lived yeast chaperone with an assembly checkpoint function that prevents premature half-proteasome dimerization until all  $\beta$  subunits are incorporated. It was the first assembly chaperone to be identified and facilitates autocleavage of the  $\beta 5$  subunit propeptide. Upon 20S maturation, it becomes the first substrate to be degraded (Ramos et al., 1998).

Other yeast chaperones such as Pba1-2 and Pba3-4 are believed to participate during early assembly events. Pba1 and Pba2 (PAC1-PAC2 in humans) bind to proteasome precursors specifically; both chaperones have C-terminal HbYX motifs that allow for specific interaction with lysines present in the pockets formed in between subunits in the  $\alpha$  ring. The archaeal ortholog of Pba1, PbaA, also binds to proteasome precursors in a HbYX motif-dependent fashion. It can be implied that the binding of these chaperones is important to prevent premature binding of activators and formation of off-pathway intermediates, and is necessary to ensure correct assembly (Hirano et al., 2005, Kusmierczyk et al., 2011, Stadtmueller et al, 2012).

$\alpha$  ring assembly is also assisted by Pba3-Pba4 in yeast (PAC3-PAC4 in humans). Pba3 and Pba4 have been shown to bind  $\alpha 5$  subunits, and are responsible for ascertaining that all  $\alpha$  subunits occupy their proper place in the  $\alpha$  ring *in vivo*. In the absence of Pba3 and/or Pba4, alternate proteasomes assemble in which an additional  $\alpha 4$  subunit takes the place of the  $\alpha 3$  subunit, yet how this occurs is not known (Kusmierczyk et al., 2008a). Our incomplete understanding of Pba3-Pba4 function is partly due to the fact that very little is known about the early events in proteasome assembly.

### 1.3.2 Self-assembly of Proteasomal Subunits

Archaeal  $\alpha$  subunits co-expressed with  $\beta$  subunits in *E. coli* form mature 20S proteasomes (Zwickl et al., 1994). Actinomycete  $\alpha$  and  $\beta$  subunits assemble into proteolytically active proteasomes in vitro (Pouch et al., 2000). Studies by Sharon et al on the assembly pathway using *E. coli* expressed *Rhodococcus erythropolis*  $\alpha$  and  $\beta$  subunits revealed the formation of  $\alpha$ - $\beta$  heterodimers, which assemble further to form half-proteasome precursors (Sharon et al., 2007). To date, no one has successfully reconstituted the assembly of eukaryotic 20S proteasomes in vitro. Such a system would greatly benefit the study of proteasome assembly but requires a much greater understanding of 20S assembly, particularly early events involving  $\alpha$  subunits.

### 1.3.3 Self-assembly of $\alpha$ subunits into Higher Order Structures

It is known that *T. acidophilum*  $\alpha$  subunits assemble into seven membered rings when expressed by themselves in *E. coli* (Zwickl et al., 1994). *Trypanosoma brucei*  $\alpha 5$  subunits assemble into heptameric rings when expressed by themselves in *E. coli* (Yao et al., 1999). Gerards et al showed that human  $\alpha 7$  subunits could not only assemble into heptameric rings when expressed by themselves in *E. coli*, but also could recruit neighboring  $\alpha$  subunits, such as  $\alpha 1$  or  $\alpha 6$ , into higher order  $\alpha$  subunit ring structures, even though these neighboring subunits could not form rings on their own (Gerards et al 1997, Gerards et al 1998). This observed dependence of  $\alpha 7$ 's neighbors on  $\alpha 7$  for assembly argues that  $\alpha$  subunits likely follow an order to assemble correctly into their final heptameric ring structure. However, the fact that the multi-subunit rings observed by

Gerards et al consisted of multiple stoichiometries also suggests that additional factors may be necessary to ensure that  $\alpha$  subunits adopt the single, correct orientation found in vivo.

In an attempt to check if similar self-assembly properties existed in yeast, individual *S. cerevisiae*  $\alpha$  subunits were expressed in *E. coli*. It was observed, however, that these subunits were mostly insoluble (Kusmierczyk unpublished). Hence, a different approach was attempted by co-expressing combinations of neighboring  $\alpha$  subunits in *E. coli*. It was thought that having two (or more) subunits that are normally neighbors in the ring may result in stabilizing interactions and improve solubility. It was observed that among the pairwise combinations tried, co-expression of  $\alpha 3$ - $\alpha 4$ , and  $\alpha 7$ - $\alpha 1$  pairs yielded soluble  $\alpha$  subunits. Interestingly, co-expression of  $\alpha 1$  and  $\alpha 7$  also resulted in the formation of a high molecular weight complex. By extending on the  $\alpha$  ring towards two more neighboring  $\alpha$  subunits, i.e.  $\alpha 5$  and  $\alpha 6$ , different combinations of  $\alpha 5$ ,  $\alpha 6$ ,  $\alpha 7$  and  $\alpha 1$  were co-expressed. It was found that every time  $\alpha 7$  and  $\alpha 1$  were present, high molecular weight complexes were observed, implying that  $\alpha 7$  and  $\alpha 1$  together could have the property to nucleate  $\alpha$  subunit assembly into higher order structures (Kusmierczyk unpublished). Co-expression of  $\alpha 5$ ,  $\alpha 6$ ,  $\alpha 7$  and  $\alpha 1$  resulted in soluble  $\alpha$  subunits and the formation of a unique, highly stable high molecular weight complex (HMWC). Mass spectrometric analysis of this complex revealed a molecular weight of  $\sim 457$  kDa, and EM analysis revealed ring like structures (Stengel and Kusmierczyk, unpublished).

## 1.4 Objectives

My studies on proteasome assembly are propelled by these questions – What happens prior to formation of the earliest known intermediate, the 15S complex, that consists of an  $\alpha$  ring and early  $\beta$  subunits? How does  $\alpha$  ring formation occur? What is/are the function(s) of Pba3-Pba4 in proteasome assembly? The aims of my project are twofold –

### **1. Characterize the HMWC formed when $\alpha 5$ , $\alpha 6$ , $\alpha 7$ , $\alpha 1$ are co-expressed in *E. coli*.**

The ease with which high molecular weight complexes, containing  $\alpha 7$  and its neighbors, are formed when either yeast or mammalian subunits are expressed in *E. coli* leads to a number of questions. What is the nature of these complexes? Are they simply dead-end complexes, or might they be assembly intermediates? And why have they not been isolated from cells, if they form so easily in recombinant form? Experiments were designed in order to:

- determine if this HMWC is a single or double ring
- understand the stoichiometry of the ring complex
- deduce the orientation of the subunits relative to each other.

Knowledge about this complex's structure can give us a better understanding of how  $\alpha$  subunit assembly occurs normally (or abnormally). It will also lead the way to determining if this, and other complexes, could represent dead-end species whose assembly must be prevented in vivo, or if they are part of putative alternate proteasome

assembly pathways. Characterization of this high molecular weight complex (HMWC) will also facilitate the second aim described below.

## **2. Determine if this complex (or similar HMWCs) exist in yeast cells.**

We know from previous studies (Yao et al., 1999, Gerards et al 1997, Gerards et al 1998) and confirmed here, that eukaryotic  $\alpha$  subunits readily give rise to non-canonical rings when expressed recombinantly, while under normal circumstances in vivo, such complexes are not observed. Perhaps this is because when all  $\alpha$  subunits are present, specific subunit interactions guide the subunits to give a specific, and correct, assembly order. It could also be due to factors that prevent non-specific interactions, such as dedicated assembly chaperones. Intriguingly, the HMWC formed when  $\alpha 5$ ,  $\alpha 6$ ,  $\alpha 7$ ,  $\alpha 1$  are co-expressed in *E. coli* is prevented from forming in the presence of Pba3-Pba4 (Chew and Kusmierczyk, unpublished). Thus, perhaps in the absence of this assembly factor in vivo, one might observe the formation of abnormal  $\alpha$  subunit complexes. The goal of this aim will be to look for this (or similar) complex(es) in *pba3* $\Delta$  and *pba4* $\Delta$  yeast cells guided by the knowledge gained about the structure of this complex from Aim 1.

## CHAPTER 2. MATERIALS AND METHODS

### 2.1 Cloning and Transformation

The plasmids used in this study are listed in Table 2. Plasmid DNA was incubated with competent BL21 cells on ice for 5 minutes. Heat-shock treatment was provided by incubation at 42 °C for 45 seconds, followed by snap cooling on ice for 5 minutes. 1 ml of LB medium was added and the mixture was incubated at 37 °C for 45 minutes with continuous shaking at 180 RPM. The cells were then pelleted and re-suspended in 50 µl of media. The re-suspended cells were spread on an LB agar plate containing 100 µg/ml ampicillin or 50 µg/ml kanamycin. The plate was incubated for 12 hrs at 37 °C to allow colony growth.

### 2.2 Protein Induction

The plasmids used in this study were transformed in BL21 cells, inoculated in 6 ml LB medium containing 100 µg/ml of ampicillin and incubated at 30 °C with vigorous shaking till the OD<sub>600</sub> reached 0.6. Protein expression was induced by isopropyl β-D-thiogalactoside (IPTG) to a final concentration of 1mM. The culture was then incubated at 30 °C with vigorous shaking for 4 hrs. Cells were harvested by repeated centrifugation at 12 000 × g for 1 min. Where protein expression was low, induction was carried out in

larger volumes (25 ml - 50 ml culture volume) and/or under lower temperature (25 °C). Cell pellets were stored at -80 °C for future use.

### 2.3 Bacterial Lysis and Protein Purification

Cell pellets were lysed using 0.6 ml – 1 ml of lysis buffer which consists of Buffer A (50 mM Hepes-NaOH, pH 7.5, 300 mM NaCl, 5 mM MgCl<sub>2</sub>), 10 µg/mL DNaseI, 300 µg/mL lysozyme, 0.1% (v/v) Triton X-100 and 2 mM pefabloc (Pentapharm), under constant shaking for 30 min. The resulting suspension is the total lysate (T), which was centrifuged at 11000 × g to give a pellet fraction (P) and supernatant, termed the soluble fraction (S). The his-tagged proteins of interest present in the soluble fraction were purified either by Ni-NTA chromatography using His SpinTrap nickel-ion columns, as per manufacturer's protocol (GE Healthcare), or by immobilized metal affinity chromatography (IMAC) using TALON His Tag Purification resin charged with cobalt (Clontech). The soluble fraction (S) was applied to 50 µl of TALON resin equilibrated with Buffer A and incubated at 4 °C with gentle rocking to enable good protein binding. This suspension was centrifuged at 700 × g for 5 min. The supernatant from this spin was aspirated and saved as flow through (F). The resin was then washed twice with Buffer A, twice with Buffer B (Buffer A with 5 mM Imidazole) and once with Buffer C (Buffer A with 10 mM Imidazole). Each wash step was carried out with the application of 1ml of the aforementioned buffers to the resin, incubation with gentle rocking for 5 min at 4 °C, and centrifugation at 700 × g for 5 min, following which the supernatant was aspirated. Finally, proteins were eluted from the resin using Elution

Buffer that consisted of Buffer A with 200 mM Imidazole. Protein concentration of the eluate (E) was determined using Pierce BCA Protein Assay Kit (from Thermo Scientific).

#### 2.4 Protein Expression Profiling

To analyze overexpression of desired proteins, following bacterial lysis, fractions of total lysate, pellet, soluble lysate, flow through and eluate were mixed with 5×Laemmli Sample Buffer to a final concentration of 1X, boiled for 10 min and stored. These fractions were analyzed by 12 % SDS-PAGE, and visualized using GelCode Blue stain (from Thermo Scientific).

#### 2.5 Native PAGE Analysis

Following purification of the proteins, the eluate fractions were analyzed by 5% native polyacrylamide gels. Eluate fractions were also analyzed using 4-15% Mini-PROTEAN TGX precast polyacrylamide gels (Bio-Rad). 5×Laemmli Buffer without SDS was added to these eluates. The electrophoretic run was at 55 V, 4 °C until the dye front ran off the gel, with standard proteins (Amersham High Molecular Weight Calibration Kit) as reference. Gels were stained using GelCode Blue.

#### 2.6 Detection of Cross-linked Bands

The eluate fractions of AKB80, AKB752, AKB753, AKB754 after purification were cross-linked in the presence of 200 μM CuCl<sub>2</sub> as described previously (Kusmierczyk et al., 2008), mixed with 5×Laemmli Buffer to a final concentration of 1X, with or without DTT, and analyzed by SDS-PAGE. The cross-linked samples were also probed

with MCP72 antibody that detects  $\alpha 7$  subunit (Enzo LifeSciences). Since this procedure yielded results with high background noise, further experiments were conducted on constructs in which internal cysteines in individual subunits were eliminated, and under varying  $\text{CuCl}_2$  concentrations.

In order to visualize the presence of cross-linked species in the eluate fraction right after purification, 20  $\mu\text{g}$  of the eluates were loaded on large 10 % SDS polyacrylamide gels, and stained using GelCode Blue. If a band was present at a position where a cross-linked band is expected, it was excised from the gel to elute the protein for further analysis. A protein band thus excised was carefully cut into finer smaller pieces, mixed with 5 $\times$ Laemmli Sample Buffer (with or without DTT) and 1 $\times$ SDS Running Buffer, then boiled for 10 min and kept at 4  $^\circ\text{C}$  overnight. The eluates and/or gel slices from this procedure were analyzed under reducing and/or non-reducing conditions on 12% SDS polyacrylamide gels, which were stained using Pierce Silver Stain Kit (from Thermo Scientific).

Similarly, in order to visualize the presence of cross-linked species in the native complexes of the various mutants under study,  $\sim 20 \mu\text{g}$  of the eluates were analyzed on native polyacrylamide gels stained with GelCode Blue. The high molecular weight complexes that were apparent upon staining were excised from the native gel; proteins from these excised bands were eluted and analyzed as described above.

## 2.7 Reversibility of Cross-linking

To demonstrate reversibility of cross-linking, cross-linked samples were first reduced with DTT to break the disulfide bonds. The DTT-treated samples were applied to PD MiniTrap G-25 columns (GE Healthcare Life Sciences) to remove the DTT. These columns were equilibrated with Buffer A prior to sample addition. The resulting eluate from each column was applied to TALON resin, also equilibrated with Buffer A, and incubated for 1 hr at 4 °C; the suspension was centrifuged at  $700 \times g$  for 5 min and the supernatant from this spin was aspirated. The proteins were then eluted using Elution Buffer, and their concentration was determined as before. Approximately 20  $\mu\text{g}$  protein from these samples were analyzed on 10 % SDS PAGE.

## CHAPTER 3 RESULTS AND DISCUSSION

### 3.1 Higher Order Complexes of *S. cerevisiae* $\alpha$ subunits

Proteasome assembly is a rapid and highly sequential process that occurs through a series of intermediates (Kunjappu and Hochstrasser, 2014). While the quest to understand the exact process of assembly is ongoing, there remains an incomplete understanding of what happens early on during the process, prior to the involvement of the  $\beta$  subunits (Figure 2). Archaeal  $\alpha$  subunits from *T. acidophilum* and  $\alpha 7$  subunits from humans not only self-assemble into heptameric rings when expressed in *E. coli*, they also form higher order structures (Zwickl et al., 1994; Gerards et al., 1998). Higher order ringed structures are also observed with recombinant  $\alpha 5$  from *Trypanosoma brucei* (Yao et al., 1999). Additionally, human  $\alpha 7$  could incorporate itself and its native neighbors into higher order structures of different stoichiometries (Gerards et al., 1998). The ability of  $\alpha$  subunits to assemble into non-canonical structures implies that eukaryotic proteasome assembly is a highly complex process that needs to be well regulated in order that correct assembly occurs.

Preliminary work in the Kusmierczyk lab sought to investigate if similar properties of self-assembly existed in *S. cerevisiae*. Individual  $\alpha$  subunits were expressed in *E. coli*, however the subunits were almost entirely insoluble. So, neighboring pairs of  $\alpha$

subunits were co-expressed with the hope that this strategy may improve solubility, and it was found that co-expression of  $\alpha 3$ - $\alpha 4$  and  $\alpha 7$ - $\alpha 1$  conferred partial solubility (Kusmierczyk, unpublished). When  $\alpha 7$  and  $\alpha 1$  were co-expressed with their native neighbors,  $\alpha 5$  and  $\alpha 6$ , in different combinations, soluble high molecular weight complexes were formed every time  $\alpha 7$  and  $\alpha 1$  were present. Specifically, co-expression of  $\alpha 5$ ,  $\alpha 6$ ,  $\alpha 7$  and  $\alpha 1$  resulted in the formation of a highly unique, soluble high molecular weight complex (HMWC). Electron microscopy analysis of this HMWC revealed the presence of rings (Kusmierczyk, unpublished). These findings indicate that *S. cerevisiae*  $\alpha$  subunits in *E. coli* can indeed self-assemble into higher order ring structures.

These captivating results suggested that it would be worthwhile to characterize this complex. The ease with which this complex forms leads one to wonder if such a complex could be an assembly intermediate, or an off-pathway (or dead-end) complex? If it is the former, how does it fit into the assembly mechanism? If it is the latter, how is its formation prevented/avoided in vivo? In either case, could one detect this species in vivo?

In order to understand the nature of this HMWC, one must first address a number of basic questions about its structure that remain outstanding. Firstly, does this HMWC form double rings as do archaeal  $\alpha$  subunits or human  $\alpha 7$  subunits? Secondly, how many subunits could be present in a ring? Thirdly, what is the order of subunits within a ring? Characterization of this complex can provide us with information necessary to look for these complexes, if formed, in vivo.

With regards to ring number, preliminary data favors the presence of two rings.  $\alpha$  subunits are similar in size (6 kDa range in yeast). The average molecular weight of  $\alpha 5$ ,  $\alpha 6$ ,  $\alpha 7$  and  $\alpha 1$  is 28.4 kDa, and a heptameric ring comprised of such an “average” subunit would be ~199 kDa. However, preliminary mass spectrometric (MS) analysis of the  $\alpha 5\alpha 6\alpha 7\alpha 1$  HMWC complex revealed a molecular weight of ~457 kDa (Stengel and Kusmierczyk, unpublished). To determine if the HMWC formed by  $\alpha 5$ ,  $\alpha 6$ ,  $\alpha 7$  and  $\alpha 1$  was a double ringed structure, we decided to start our investigations using the archaeal system, wherein there is only one type of  $\alpha$  subunit and double ring formation has been studied previously, with the hope of extending findings from these studies to understand double ring formation in *S. cerevisiae*.

### 3.2 Formation of $\alpha$ - $\alpha$ Double Rings in Archaea

When *T. acidophilum*  $\alpha$  subunits were expressed in *E. coli*, it was reported that they mostly formed  $\alpha$ - $\alpha$  double heptameric rings, and a very small fraction of single heptameric rings were observed (Zwickl et al., 1994). Our lab studies the proteasome from the archaeon *Methanococcus maripaludis* as a model. In an attempt to see whether double ring formation occurs with *M. maripaludis*, we expressed *M. maripaludis*  $\alpha$  subunits (AKB191) in *E. coli*.  $\alpha$  subunits from *T. acidophilum* (AKB780) were used as reference. A hexahistidine tag (his tag) was incorporated at the C-terminus of  $\alpha$  subunits to enable purification by immobilized metal affinity chromatography (IMAC).  $\alpha$  subunits thus purified were analyzed by native PAGE. A single *M. maripaludis*  $\alpha$  subunit has a size of 28.5 kDa (pI 5.03), while that of *T. acidophilum* is 25.8 kDa (pI 5.5). We observed that *M. maripaludis*  $\alpha$  subunits migrate as two species, a major species of higher

electrophoretic mobility and a minor species of lower mobility (Figure 3). The position of the two *M. maripaludis* bands relative to the double-ringed *T. acidophilum*  $\alpha$  subunit complexes and the molecular size standards is consistent with the lower band corresponding to a single-ring species and the upper band corresponding to a double ring species. It is, however, not known how double rings interact with each other.

If one were to observe the 20S proteasome core from inside, the surface of  $\alpha$  subunits at the  $\alpha$ - $\beta$  interface appears to be rugged in comparison to the surface at the top of the  $\alpha$  ring that faces outside, which is relatively smooth (Figure 4a). Theoretically, if two  $\alpha$  rings were to come together, there are three possible ways in which it could happen – one, the smooth surfaces of both rings would be proximal (Figure 4b), two, the rugged surfaces of both rings would be proximal (Figure 4c), and three, the rugged surface of one ring would be proximal to the smooth surface of the other (Figure 4d). Electron microscopy findings suggest that *T. acidophilum*  $\alpha$ - $\alpha$  rings are not in alignment but have a rotational offset angle of  $25^\circ$  with respect to each other (Zwickl et al., 1994). This is similar to the  $25^\circ$  offset between  $\alpha$ - $\beta$  rings of a mature proteasome (Lowe et al., 1995). Given that  $\alpha$  and  $\beta$  subunits share nearly identical folds, this would suggest that  $\alpha$ - $\alpha$  rings have a similar structure to  $\alpha$ - $\beta$  rings. Therefore, we hypothesize that  $\alpha$ - $\alpha$  rings are likely to be positioned with the rugged surfaces of both rings in close proximity (as shown in Figure 4c). The resolution of the electron micrographs was not sufficient to permit the determination of this positioning (Zwickl et al., 1994). Therefore, we set out to test this hypothesis.

The crystal structure of the 20S proteasome from *T. acidophilum* reveals the presence of an  $\alpha$  helix (H1) in both  $\alpha$  and  $\beta$  subunits that contributes to the  $\alpha$ - $\beta$  interface between rings (Lowe, 1995) (Figure 5). Since  $\alpha$  and  $\beta$  subunits have nearly identical folds, we hypothesized that this  $\alpha$  helix also contributes to the  $\alpha$ - $\alpha$  interface when two  $\alpha$  subunits sit across each other in a double ring. To test this hypothesis, we compared the relative positioning of the two opposing (or anti-parallel) H1 helices and surmised that a cysteine residue introduced at position 99, in the H1 helix of one *M. maripaludis*  $\alpha$  subunit, would be in a suitable position to form a cross-link with an identical cysteine at position 99 in the H1 helix of an opposing  $\alpha$  subunit. We generated the Q99C mutant alpha subunit (AKB600), expressed it in *E. coli*, and purified it by IMAC. The partially purified mutant protein was subjected to native and SDS-PAGE along with a similarly isolated wild-type protein (AKB191). As before, the wild-type  $\alpha$  subunit migrated as two species on native PAGE, a faster-migrating major species (which we proposed to be a single ring) and a slower-migrating minor species (which we proposed to be a double ring). However, in the Q99C mutant, we observed efficient, essentially complete, transition from the faster-migrating species to the slower migrating species (Figure 6a). This is consistent with a shift into the double ring (i.e. cross-linked) form. The shift to the putative double ring form was also observed in a Q99C mutant in which the three endogenous cysteines present in the  $\alpha$  subunit were replaced with alanines (AKB709). By contrast, a mutant without any cysteines present (AKB708) behaved essentially like the wild-type protein on native PAGE (Figure 6a). This argued that the transition was dependent on the introduced cysteine at position 99, and was not a consequence of crosslinking between native cysteine residues present in the  $\alpha$  subunit. The presence of

cross-linking was confirmed when the purified samples were subjected to non-reducing SDS-PAGE (Figure 6b). A prominent  $\alpha$ - $\alpha$  dimer band of  $\sim 57$  kDa in size was observed in the AKB709 sample and, to a much lesser extent, the AKB600 sample. Both of these contain the Q99C mutation, but the endogenous cysteines are still intact in AKB600 which perhaps explains the lower specific cross-linking efficiency (see below). No  $\alpha$ - $\alpha$  dimer band was observed in the AKB708 mutant that contained no cysteines at all. The dimer bands were not observed under reducing conditions (Figure 6c), confirming that they were caused by disulfide crosslinks.

Although the presence of the  $\alpha$ - $\alpha$  dimer bands in the two Q99C mutants (AKB600 and AKB709) on non-reducing SDS-PAGE (Figure 6b) correlates with the observed transition to the putative ring dimer band that these two mutants display on native PAGE (Figure 6a), we still must demonstrate that the  $\alpha$ - $\alpha$  dimer band is present in the putative ring dimer band. To this end, purified archaeal proteins from AKB191, AKB600, and AKB709 were subjected to native PAGE (Figure 7a). The putative double ring complex bands were excised (indicated by arrow in Figure 7a) and the proteins therein eluted. The eluates were analyzed under reducing and non-reducing conditions by SDS-PAGE (Figure 7b). Cross-linked bands were again observed in AKB600 and AKB709 under non-reducing, but not under reducing, conditions. This confirmed that the cross-linked  $\alpha$ - $\alpha$  dimer bands were present in the gel shifted species and that the Q99C mutation was responsible for the gel shift to the slower migrating, putative ring dimer band.

The degree of crosslinking in the native complexes was again greater in AKB709 than in AKB600, as can be seen from the intensity of the cross-linked bands on the silver-stained gel in Figure 7b. We believe this is because AKB600 contains the 3 endogenous cysteines, while AKB709 does not. The presence of these additional cysteines might decrease the efficiency of formation of the specific Q99C crosslinks by forming non-specific inter- and intra-molecular crosslinks which can lead to subunit multimerization. Evidence for this is seen Figure 7b where the AKB600 sample accumulates high molecular weight species that migrate above the  $\alpha$ - $\alpha$  dimer band. These species disappear upon DTT addition, arguing that they are cysteine-based. An additional question pertains to why the extent of the transition to the putative ring dimer band on native PAGE is the same for both AKB600 and AKB709 if the efficiency of formation of the specific Q99C crosslink is so much smaller in AKB600? This is most likely because only one pair of cross-linked  $\alpha$  subunits is necessary to hold a double ring together.

In our final analysis, we introduced a cysteine just one position on either side of Q99 in the H1 helix. We surmised that if cross-linking is dependent on the precise apposition of two opposing (or anti-parallel) H1 helices, then even minor alterations in the placement of the cross-linkable cysteine should decrease the efficiency of cross-linking. We generated an A98C mutant  $\alpha$  subunit (AKB706) and an M100C mutant  $\alpha$  subunit (AKB707) and purified them as before. Native PAGE analysis of these proteins reveals considerably less double ring species being formed in the M100C mutant relative to the Q99C mutant while the A98C mutant appeared indistinguishable from wild-type

(Figure 8). Hence precise positioning of the cross-linkable cysteine on  $\alpha$  subunits is necessary to effect efficient double ring formation.

Taken together, these experiments allow us to reach three important conclusions. First, these experiments show that *M. maripaludis*  $\alpha$  subunits are also capable of forming double rings and confirm our initial assignment of bands on native PAGE (i.e. lower band as the single ring, upper band as the double ring, Figure 3). Second, the experiments support our hypothesis that a double ring of  $\alpha$  subunits is structurally similar to a half-proteasome (i.e. an  $\alpha$ - $\beta$  ring pair) and forms via the apposition of two rugged surfaces (Figure 4c). This represents the first biochemical evidence for the orientation of rings in an  $\alpha$  ring dimer. Finally, introducing a cross-linkable cysteine in the H1 helix is useful to detect the presence of  $\alpha$  subunits across each other in a double ring and can be employed to study the structure of other double  $\alpha$  rings, such as the possible double rings of the HMWC containing yeast  $\alpha 5$ ,  $\alpha 6$ ,  $\alpha 7$  and  $\alpha 1$ .

### 3.3 Crosslinking Analysis of AKB80 ( $\alpha 5\alpha 6\alpha 7\alpha 1$ -his) and its Mutants

We adopted the strategy of crosslinking to characterize the AKB80 ( $\alpha 5\alpha 6\alpha 7\alpha 1$ -his) complex. We proposed to introduce cysteine residues in the H1 helix of each  $\alpha$  subunit corresponding to position 99 in the *M. maripaludis*  $\alpha$  subunit. From ClustalW sequence alignment of the different  $\alpha$  subunits (Figure 9), we proposed the following mutations -  $\alpha 5$ (V97C),  $\alpha 6$ (N93C),  $\alpha 7$ (A97C) and  $\alpha 1$ (A102C). Using AKB80 ( $\alpha 5\alpha 6\alpha 7\alpha 1$ -his) as template, different combinations of these mutants were generated in the hope that cross-linking of  $\alpha$  subunits could then be detected.

Since high molecular complexes were readily formed whenever  $\alpha 7$  and  $\alpha 1$  were present together (recall section 1.3.3), we initiated creating constructs by introducing in AKB80, mutations in  $\alpha 7$ (A97C) and/or  $\alpha 1$ (A102C) to generate AKB752 ( $\alpha 5\alpha 6\alpha 7$ (A97C) $\alpha 1$ -his), AKB753 ( $\alpha 5\alpha 6\alpha 7\alpha 1$ (A102C)-his) and AKB754 ( $\alpha 5\alpha 6\alpha 7$ (A97C) $\alpha 1$ (A102C)-his). These mutants were expressed in *E. coli*, and purified using his-tag based IMAC. Their expression was profiled by SDS-PAGE demonstrating our ability to successfully produce the mutant proteins (Figure 10). The purified proteins were cross-linked in the presence of 0.2 mM  $\text{CuCl}_2$  and analyzed by SDS-PAGE under reducing (600 mM DTT) and non-reducing conditions (Figure 11a). The cross-linked samples were also probed with MCP72 antibody that detects  $\alpha 7$  subunit (Figure 11b). In the absence of DTT, the proteins are exposed to a non-reducing environment where cross-linking is induced by the addition of  $\text{CuCl}_2$ . The relative molecular masses for these four subunits range between 25.5 kDa ( $\alpha 6$ ) and 31.5 kDa ( $\alpha 7$ ), with an average MW of 28.4; a cross-linked dimer would be in the 50-60 kDa range. Addition of DTT reduces the disulfide bond, if present, and the  $\alpha$  subunits can be seen at their respective monomeric positions only. If  $\alpha 7$  cross-linked with itself via C97, a unique band, not present in control (AKB80 with no cross-linkable cysteines), would show up in both AKB752 and in AKB754 lanes. Similarly, if  $\alpha 1$  cross-linked with itself via C102, a unique band, not present in control (AKB80), would show up in both AKB753 and in AKB754 lanes. If  $\alpha 7$  and  $\alpha 1$  are cross-linked, a unique band would show up in AKB754 lane only. We observed that  $\alpha$  subunits had a tendency to cross-link with each other, as can be seen by the presence of bands around 50 kDa. However, the presence of such bands even in the control lane (AKB80) implied that the internal cysteine residues of  $\alpha$  subunits also

participated in cross-linking, as was likely the case with the archaeal  $\alpha$  subunits. This made it difficult to visualize unique bands in the experimental lanes, necessitating the removal of internal native cysteines.

### 3.3.1 Resolving the Noise Caused by Native Cysteines

Internal cysteines are present in  $\alpha 5$  (residues 76, 117, 221),  $\alpha 6$  (residues 66, 92, 113),  $\alpha 7$  (42, 76, 219), and in  $\alpha 1$  (residues 50, 74, 114). We generated constructs such that the genes for each subunit that would bear the cross-linkable H1 helix cysteine would have no internal cysteines. It was hoped that this would help reduce background cross-linking described above. Therefore the next set of constructs that were created were AKB786 ( $\alpha 5\alpha 6\alpha 7$ (A97C, no internal cysteines) $\alpha 1$ -his), AKB788 ( $\alpha 5\alpha 6\alpha 7\alpha 1$ (A102C, no internal cysteines)-his) and AKB789 ( $\alpha 5\alpha 6\alpha 7$ (A97C, no internal cysteines) $\alpha 1$ (A102C, no internal cysteines)-his). Pilot experiments to test initial expression and solubility of these constructs revealed that  $\alpha$  subunits failed to solubilize when  $\alpha 7$  was mutated to  $\alpha 7$ (A97C, no internal cysteines) and the protein yield was low in comparison to AKB80 when  $\alpha 1$  was mutated to  $\alpha 1$ (A102C, no internal cysteines) (data not shown). To rectify this issue, the proteins were expressed at room temperature (25 °C) in 25 ml cultures, which improved solubility and yield.

Once the troubleshooting was completed, cross-linking experiments were carried out as described earlier, with purified proteins of AKB80, AKB786, AKB788 and AKB789. The samples were cross-linked with 0.2 mM  $\text{CuCl}_2$  and analyzed by SDS-PAGE. Cross-linked samples were also probed with MCP72 (to detect  $\alpha 7$ ) and anti-his antibody (to detect  $\alpha 1$ ) (Figure 12). Under non reducing conditions, if crosslinking of the

subunits were to occur via the cross-linkable cysteine uniquely, the cross-linked bands would appear between 51 kDa - 63kDa. Although we were able to visualize bands in lanes AKB786, 788, 789 (Figure 12), it was difficult to determine if they were unique owing the high level of background bands still present in the AKB80 control. Using AKB80 as control could result in higher background levels owing the internal cysteines still being present. Therefore, cross-linking experiments were proposed to be repeated with constructs AKB80, AKB786, AKB788, AKB789 and their new respective controls AKB785 ( $\alpha 5\alpha 6\alpha 7$ (no cysteines) $\alpha 1$ -his), AKB787 ( $\alpha 5\alpha 6\alpha 7\alpha 1$ (no cysteines)-his), and AKB796 ( $\alpha 5\alpha 6\alpha 7$ (no cysteines) $\alpha 1$ (no cysteines)-his). However, making these additional mutations presented its own set of problems. For instance, the protein yield of AKB787 was extremely low even after scaling up cultures (data not shown); hence we were forced to resort to rely on AKB80 as control.

### 3.4 Cross-linking Analysis of AKB80 ( $\alpha 5\alpha 6\alpha 7\alpha 1$ -his) in Purified Eluates

We had thus far created constructs that removed the internal cysteine residues on a particular  $\alpha$  subunit whenever we introduced a cross-linkable cysteine into that subunit, as in the case of AKB786, AKB788 and AKB789. The other  $\alpha$  subunits on these constructs were not mutated so as to keep the mutations to a minimum. However the internal cysteine residues present on them could still contribute towards crosslinking and give rise to the background that we were observing even in our AKB80 control. To reduce background, we wondered if we could spot the specific cross-linked bands in the purified eluates without the aid of  $\text{CuCl}_2$  to effect crosslinking. The reason we employed  $\text{CuCl}_2$  in the first place was due to previous work with engineered cross-linkable

cysteines in yeast proteasome subunits that successfully used this metal to induce oxidizing conditions (Velichutina et al., 2004; Kusmierczyk et al., 2008b). However, our purification buffers do not contain DTT, and our purification scheme uses IMAC, which exposes the protein to redox reactive divalent cations such as nickel and cobalt. Perhaps these conditions were sufficiently oxidizing to allow specific crosslinks to form without the need for exogenous  $\text{CuCl}_2$ . This was already shown to be the case with the archaeal subunits, whose Q99C crosslinks did not require the addition of  $\text{CuCl}_2$  (Figure 6b).

#### 3.4.1 Analysis with Cross-linkable Cysteine in $\alpha 1$

To test our new experimental scheme, we expressed the AKB80 control construct containing wild-type  $\alpha$  subunits and the mutant AKB788 construct. We purified the proteins using IMAC as before and analyzed the purified eluates by SDS-PAGE under non-reducing conditions (Figure 13). A prominent band was present in the purified eluate of AKB788 at a height slightly above 50 kDa, which was absent in the purified elute of AKB80 (L1 and L2, Figure 13). Upon providing reducing conditions, i.e. addition of 1mM DTT, this band disappeared (L4 and L5, Figure 13). When these reduced samples were re-subjected to oxidizing conditions (via removal of DTT using desalting columns and reapplication to IMAC resin charged with cobalt) the prominent band from L2 re-appeared (L7 and L8, Figure 13). These observations imply that the prominent band in AKB788 is a cross-linked band that presents itself under non-reducing conditions.

In order to see what the cross-linked band from the purified eluate of AKB788 contained, the cross-linked bands from L2 and L8 in Figure 13 were excised from the gel, and the proteins were eluted in the presence of 600 mM DTT. These eluates were

analyzed on SDS-PAGE and visualized by silver staining. The presence of a prominent band migrating in L4 and L6 (Figure 14) at a size comparable to  $\alpha 1$  in the control lane implies that the major species in the excised bands has  $\alpha 1$  cross-linked to  $\alpha 1$ , via the introduced cross-linkable cysteine in helix H1.

### 3.4.2 Analysis with Cross-linkable Cysteine in $\alpha 7$

The purified eluate of AKB786 ( $\alpha 5\alpha 6\alpha 7$ (A97C, no internal cysteines) $\alpha 1$ -his), was analyzed by SDS-PAGE under reducing (1mM DTT) and non-reducing conditions using AKB785 ( $\alpha 5\alpha 6\alpha 7$ (no cysteines) $\alpha 1$ -his), as control. No unique bands were observed in AKB786 (L2, Figure 15) despite repeated trials. If crosslinking were to occur, one would expect to have obvious results as seen with AKB788 or with AKB709. Since the same procedures on AKB786 do not present any such obvious bands, a more sensitive method of detection may need to be employed to probe for possible crosslinking. An alternate possibility is that perhaps the positioning of the cross-linkable cysteine in  $\alpha 7$  is not ideal to bring about most efficient crosslinking. We saw with the archaeal a subunit that changing the positioning of the cysteine by just one residue greatly diminished cross-linking efficiency (Figure 8). Our choice of which residue to mutate was based on a simple alignment (Figure 9) of H1 helix sequences. But alignment of primary sequence may not always imply identical positioning in three dimensional space of the residue in question. Finally, it could also be possible that there is, after all, no crosslinking between  $\alpha 7$  and itself despite the presence of a cross-linkable cysteine in  $\alpha 7$ . Whatever the case may be, more experiments are needed before one can rule out that there is no crosslinking in case of AKB786.

### 3.4.3 Analysis with Cross-linkable Cysteine in $\alpha 7$ and $\alpha 1$

A cross-linkable cysteine is present in both  $\alpha 7$  and  $\alpha 1$  in AKB789 ( $\alpha 5\alpha 6\alpha 7$ (A97C, no internal cysteines) $\alpha 1$ (A102C, no internal cysteines)-his). We used AKB796 ( $\alpha 5\alpha 6\alpha 7$ (no cysteines) $\alpha 1$ (no cysteines)-his) as control. The purified eluates of AKB796 and AKB789 were analyzed by SDS-PAGE. Under non-reducing conditions, three bands (indicated as A, B and C) were distinctly visible between 50 and 75 kDa in AKB789 and were not present in the control lane (L1 and L2, Figure 16). These bands disappear when the eluates are treated with 1 mM DTT, implying that they are disulfide cross-linked bands (L4 and L5, Figure R16). When 50  $\mu$ M  $\text{CuCl}_2$  was added to the reduced samples (purified eluates treated with 1 mM DTT), re-appearance of the cross-linked bands can be observed, albeit to a lesser degree (L7 and L8, Figure 16).

In order to see what the cross-linked bands from the purified eluate of AKB789 contained, the cross-linked bands were excised from the gel; the proteins from these bands were eluted in the presence of 600 mM DTT and analyzed on SDS-PAGE and visualized by silver staining. Eluate from Band A shows the presence of a prominent band (L4, Figure 17) migrating at a size comparable to  $\alpha 1$  in the control lane. This implies that the major species in Band A has  $\alpha 1$  cross-linked to  $\alpha 1$ , via its cross-linkable cysteine. No  $\alpha$  subunits were detected in eluates from the other bands i.e. Band B and Band C (L6 and L8, Figure 17). Perhaps the amount of protein that was eluted from these bands was too low to be detected by silver staining. Further experimentation is necessary to ascertain what these band constitute.

### 3.5 Cross-linking Analysis of AKB80 ( $\alpha 5\alpha 6\alpha 7\alpha 1$ -his) in Native Complexes

The above analyses demonstrated the presence of cross-linked bands present in the IMAC-purified eluates. However, it remained to be seen if these cross-linked species were present in assembled the HMWC. To this end, we undertook a similar analysis to that carried out with archaeal  $\alpha$  subunits (Figure 7).

#### 3.5.1 Analysis with Cross-linkable Cysteine in $\alpha 1$

Proteins purified by IMAC, as before, from bacteria expressing AKB80 and AKB788 were analyzed by native PAGE (Figure 18). A single band was observed in the AKB80 sample, corresponding to the known HMWC formed by  $\alpha 5$ ,  $\alpha 6$ ,  $\alpha 7$  and  $\alpha 1$ . Interestingly, two bands were observed in the AKB788 sample, one at a mobility comparable to that of the HMWC in AKB80 (AKB788 Band 1, Figure 18), and the other at a slightly faster mobility (AKB788 Band 2, Figure 18). This implies that there are, at the least, two major species of HMWCs formed in AKB788. To check whether these native complexes in AKB788 had any cross-linked  $\alpha$  subunits, the HMWC bands were excised and the proteins eluted. The eluates were analyzed by SDS-PAGE under non-reducing conditions. A prominent band was observed in the gel-slice eluates of AKB788 Native Band 1 and 2 (L5, L6, Figure 19a) slightly above 50 kDa, running at a height comparable to the previously observed cross-linked band in purified eluates of AKB788 (L2, Figure 19a) that we know contained  $\alpha 1$  disulfide linked to itself. Importantly, this band was not present in the AKB80 control lanes (L1 and L4, Figure 19a). The prominent ~50 kDa bands from both L5 and L6 (Figure 19a) were excised, the proteins therein eluted and subjected to SDS-PAGE under reducing conditions (Figure 19b). The gel was

visualized by silver staining. It can be seen that the major species in the excised bands migrates at a height comparable to  $\alpha 1$  (L5, L6, L7, Figure 19b). Therefore the cross-linked bands consist of  $\alpha 1$  cross-linked to itself, via its cross-linkable cysteine in helix H1. We conclude that the  $\alpha 1$ - $\alpha 1$  crosslinks are present in both of the native complexes present in AKB788.

### 3.5.2 Analysis with Cross-linkable Cysteine in $\alpha 7$

Proteins purified by IMAC, as before, from bacteria expressing AKB786 and AKB785 were analyzed by native PAGE (Figure 20). As above, two bands were seen in each of the mutant samples, one at a mobility comparable to that of the HMWC present in AKB80 (AKB785 and AKB786 Band 1, Figure 20), and the other at a slightly faster mobility (AKB785 and AKB786 Band 2, Figure 20), implying the presence of, at the least, two major species of HMWCs in AKB785 and AKB786. These native complex bands were excised and the proteins eluted; the eluates were analyzed by SDS-PAGE under non reducing conditions. The gel was visualized by silver staining. No distinctly unique bands were observed in AKB786 native complexes (L6 and L8, Figure 21) that were not present in the no-cysteine controls (L2 and L4, Figure 21). This is consistent with previous results (Figure 15) showing a lack of cross-linked species present when  $\alpha 7$  contains a cross-linkable cysteine in its H1 helix. As before, the same caveats about interpreting this negative result apply (see discussion in 3.4.2).

### 3.5.3 Analysis with Cross-linkable Cysteine in $\alpha 7$ and $\alpha 1$

Proteins purified by IMAC, as before, from bacteria expressing AKB789 and AKB796 were subjected to native PAGE (Figure 22). Here too, two bands were seen in each of samples, one at a mobility comparable to that of the HMWC present in AKB80 (AKB796 and AKB789 Band 1, Figure 22), and the other at a slightly faster mobility (AKB796 and AKB789 Band 2, Figure 22), implying the presence of, at the least, two major species of HMWCs in AKB785 and AKB786. These native complex bands were excised and the proteins eluted; the eluates were analyzed by SDS-PAGE under non reducing conditions. The gel was visualized by silver staining. Distinct bands were observed in the eluates of AKB789 Native Band 1 and 2 (L5, L7, Figure 23) between 50 kDa and 75 kDa. These bands were not present in the control lanes (L1 and L3, Figure 23), and this banding pattern is comparable to the pattern of cross linked bands formed in purified eluates of AKB789 (L2, Figure 16). It is likely that Band A as observed in Figure R23 is identical to Band A observed in Figure 16. Further experimentation is required to confirm this claim, which if true, will imply that the native complexes of AKB789 too have an  $\alpha 1$ - $\alpha 1$  crosslink.

### 3.6 Identifying $\alpha 1$ - $\alpha 1$ Crosslinks in Higher Order Complexes other than of AKB80 ( $\alpha 5\alpha 6\alpha 7\alpha 1$ -his)

Our experiments thus far have established the ability of  $\alpha 1$  in the HMWC containing  $\alpha 5$ ,  $\alpha 6$ ,  $\alpha 7$  and  $\alpha 1$  to crosslink with itself in the presence of a cross-linkable cysteine. This implies that (at least) one pair of  $\alpha 1$  subunits, with each subunit located in a different ring, sit opposite each other in these double ring complexes. Our previous

work has shown that whenever yeast  $\alpha 7$  and  $\alpha 1$  were co-expressed in *E. coli*, high molecular weight complexes (HMWCs) were observed (Kusmierczyk, unpublished). Hence, attempts were initiated to check for the presence of such  $\alpha 1$ - $\alpha 1$  crosslinking in different HMWCs containing  $\alpha 7$  and  $\alpha 1$ .

When  $\alpha 7$  and  $\alpha 1$  from the AKB143 ( $\alpha 7\alpha 1$ -His) construct are co-expressed in *E. coli*, higher order structures are observed. We introduced the cross-linkable cysteine in  $\alpha 1$  to generate AKB883 ( $\alpha 7\alpha 1$ (A102C, no internal cysteines)-his) and expressed it in *E. coli*. The  $\alpha$  subunits from AKB143 and AKB883 were purified by IMAC, as before, and the purified eluates were analyzed by native PAGE. AKB143 shows the presence of a major species (Band 2, L4, Figure 24) and a slower-migrating minor species (Band 1, L4, Figure 24). A similar banding pattern is observed in AKB883 with the slower band being slightly more prominent (L7, Figure 24). Proteins from these bands were extracted and analyzed under non-reducing conditions by SDS-PAGE (Figure 25). A prominent band is present in both native complexes present in the AKB883 sample (L6, L7, Figure 25) and this band migrates at a height comparable to the  $\alpha 1$ - $\alpha 1$  cross-linked band of AKB788 (L1, Figure 25). As expected, this band is also found to be present in the purified eluate fractions of AKB883 (L3, Figure 25). We infer this band to be  $\alpha 1$  cross-linked to itself.

Similarly, when  $\alpha 6$ ,  $\alpha 7$  and  $\alpha 1$  from the AKB145 ( $\alpha 7\alpha 1$ -His) construct are co-expressed in *E. coli*, higher order structures are observed. We introduced the cross-linkable cysteine in  $\alpha 1$  to generate AKB885 ( $\alpha 6\alpha 7\alpha 1$ (A102C, no internal cysteines)-his) and expressed it in *E. coli*. The purified eluates were analyzed by native PAGE. AKB145 shows the presence of a major species (Band 1, L3, Figure 24) and a slower-migrating

minor species that migrates similar to the major species in AKB143. This slower-migrating species in AKB145 (Band 2, L3, Figure 24) was previously shown to contain  $\alpha 7$  and  $\alpha 1$ , just like the major species in AKB143, arguing that they were the same complex (Kusmierczyk, unpublished). The AKB885 sample also shows the presence of a major and minor species, just like the AKB145 sample (Band 1 and 2, L6, Figure 24). Proteins from these native complexes were extracted and analyzed under non-reducing conditions by SDS-PAGE (Figure 26). Distinct bands were present in both complexes in the AKB885 sample (which contained the cross-linkable cysteine on  $\alpha 1$ ) that were not present in the AKB145 sample. The migration of these distinct bands was comparable to that of the  $\alpha 1$ - $\alpha 1$  cross-linked band present in AKB788 (L6, L7, Figure 26); the distinct band is also present in the purified elute fractions of AKB885 (L3, Figure 26). We infer this band to be  $\alpha 1$  cross-linked to itself.

Together, experiments on AKB883 and AKB885 imply that in each HMWC containing  $\alpha 7$  and  $\alpha 1$ , there are (at least) two subunits of  $\alpha 1$ , that sit directly across from each other in each of the two rings of these double ringed complexes. Moreover, the  $\alpha 1$  with a cross-linkable cysteine on it might be able to serve as a tracker to detect such complexes in vivo.

## CHAPTER 4. CONCLUSIONS AND FUTURE DIRECTIONS

Attempts to understand the assembly of proteasomes is an ongoing and advancing process. While the order of assembly of  $\beta$  subunits has been delineated using mammalian subunits (Hirano et al, 2008), we still do not know how  $\alpha$  subunits assemble. Self-assembly of proteasomal subunits is a significant feature of proteasome assembly. While entire 20S units were found to be assembled when archaeal  $\alpha$  and  $\beta$  subunits from *T. acidophilum* were co-expressed in *E. coli* (Zwickl et al, 1994), it was also discovered that certain  $\alpha$  subunits from divergent species have a property to self-assemble into single and double heptameric rings (Yao et al., 1999, Gerards et al 1997, Gerards et al 1998). In this study, we have shown that recombinant  $\alpha$  subunits from the archaeon *M. maripaludis* also have a tendency to self-assemble into higher order structures. We found two species of high molecular weight complexes when these  $\alpha$  subunits were expressed in *E. coli* – one migrating at a position where a single ring would be present, and the other migrating at a position comparable to the double ring from *T. acidophilum*. We hypothesized that if  $\alpha$  subunits assembled into double ring forms, then subunits that are positioned across each other in the two rings could be cross-linked in the presence of a cysteine residue positioned suitably. However, the choice of where to position the cysteine would depend on the orientation of the two rings relative to each other. As mentioned before, a single heptameric  $\alpha$  ring presents two types of surfaces for interaction – a rugged surface on one

side, comparable to that found at the  $\alpha$ - $\beta$  interface, and a relatively smooth surface on the opposite side. Double  $\alpha$  rings could interact such that the two surfaces that come together are both rugged (as in  $\alpha$ - $\beta$  rings), both smooth, or are rugged and smooth (recall Figure 4). Since  $\alpha$  and  $\beta$  have very similar folds, we supposed that two  $\alpha$  rings likely interact as do  $\alpha$ - $\beta$  rings. An H1 helix is present on both  $\alpha$  and  $\beta$  subunits at an  $\alpha$ - $\beta$  interface. So, introducing a cysteine in the H1 helix of an  $\alpha$  subunit should enable cross-linking of two  $\alpha$  subunits across each other in the rings, if the double  $\alpha$  rings were to resemble  $\alpha$ - $\beta$  rings. When  $\alpha$  subunits assembled into heptameric rings, we were able to observe efficient formation of the heavier species when  $\alpha$  subunits had a cross-linkable cysteine in the H1 helix. We were also able to detect  $\alpha$ - $\alpha$  crosslinks in the heavier species of *M. maripaludis*  $\alpha$  subunits and hence we concluded that these structures were in the form of double rings. It is interesting that introducing a cross-linkable cysteine in an  $\alpha$  subunit at the H1 helix is enough to cause a complete transition to the double ring form and leads to the question of how these double rings are formed. One possibility is that single  $\alpha$  rings are formed first and exist in equilibrium with double rings. When one single ring encounters another single ring, the cysteines in the H1 helices form a disulfide bond and the two rings are held intact. The equilibrium shifts until all single rings are locked into double rings. Perhaps this is why we could observe no single ring with the Q99C mutant (AKB709) (refer Figure 6a). It could also be possible that *M. maripaludis*  $\alpha$  subunits assemble into primarily double rings, just like *T. acidophilum*  $\alpha$  subunits. However, these *M. maripaludis* double rings then fall apart into single rings upon native PAGE; crosslinking prevents this dissociation. Size exclusion chromatography can be employed to test this hypothesis and identify single rings, if present.

We have also investigated self-assembly of  $\alpha$  subunits in *S. cerevisiae* and attempted to characterize a high molecular weight complex (HMWC) that is formed upon co-expression of  $\alpha 5$ ,  $\alpha 6$ ,  $\alpha 7$  and  $\alpha 1$  in *E. coli*. EM studies of this complex suggest that it forms ring-like structures (Kusmierczyk, unpublished). Using our cross-linking strategy, we have shown that this complex is a double ring with similar relative orientation (i.e. rugged-to-rugged) of the two rings to that found in archaeal  $\alpha$  subunit rings. Using a cross-linkable cysteine placed in  $\alpha 1$ , at a position equivalent to Q99C in archaea, we detected  $\alpha 1$  crosslinking to itself implying that there are (at least) two copies of  $\alpha 1$  present, one copy per ring, which are positioned across from each other. We did not observe any cross-linked bands when we introduced a cross-linkable cysteine on  $\alpha 7$ . This is consistent with (albeit does not prove) a lack of two  $\alpha 7$  subunits positioned across from each other in the double ring. Cross-linkable cysteines were also introduced in  $\alpha 5$  and  $\alpha 6$ ; cross-linking experiments using these subunits are in progress. Further experimentation is required to specify the positioning of other  $\alpha$  subunits in this high molecular weight complex. It is also not clear how many subunits are present in each ring. MS analysis of this complex reveals a MW of  $\sim 457$  kDa, which implies that it is more likely that the rings are octameric than being heptameric (Stengel F and Kusmierczyk AR, unpublished), which is intriguing because all proteasomal subunits, until now, have only been observed to form seven membered rings. Results from additional cross-linking experiments will be used to deduce possible  $\alpha$  subunit positioning, which we hope will lead us further towards inferring the nature and stoichiometry of these rings.

By introducing a cross-linkable cysteine in  $\alpha 1$ , we were also able to detect  $\alpha 1$ - $\alpha 1$  crosslinks in high molecular weight complexes that are formed when  $\alpha 7$  and  $\alpha 1$  are co-

expressed, and when  $\alpha_6$ ,  $\alpha_7$  and  $\alpha_1$  are co-expressed in *E. coli*. The natural order of  $\alpha$  subunits in a heptameric  $\alpha$  ring of a 20S proteasome is  $\alpha_1$ - $\alpha_2$ - $\alpha_3$ - $\alpha_4$ - $\alpha_5$ - $\alpha_6$ - $\alpha_7$ .  $\alpha_7$  and  $\alpha_1$  together assemble into HMWCs with ease. Perhaps  $\alpha_7$  and  $\alpha_1$  have the ability to nucleate into modules (possibly tetrameric) in which  $\alpha_1$  is positioned across itself, and these tetrameric modules come together to form HMWCs. We observe HMWCs when  $\alpha_6$   $\alpha_7$   $\alpha_1$  are co-expressed. Perhaps  $\alpha_7$  and  $\alpha_1$  do have an ability to incorporate native neighboring subunits, and in this case, incorporate  $\alpha_6$  into the aforementioned modules in which  $\alpha_1$  is positioned across itself. We also observe HMWCs when  $\alpha_5\alpha_6\alpha_7\alpha_1$  are co-expressed. If  $\alpha_7$  and  $\alpha_1$  initially add on  $\alpha_6$ , and then add on  $\alpha_5$  into this existing module, this would result in an octameric module in which  $\alpha_1$  is positioned across itself, and two such modules come together to form the HMWC that has been under focus in this study. Indeed, MS analysis of this  $\alpha_5\alpha_6\alpha_7\alpha_1$  complex implies that these double rings are likely octameric. We do not see any single rings when  $\alpha_5\alpha_6\alpha_7\alpha_1$  are co-expressed, and this is consistent with these HMWCs being assembled through the afore-mentioned modules, and not by way of two single rings coming together.

$\alpha_7\alpha_1$  and  $\alpha_3\alpha_4$ , the two pairs of  $\alpha$  subunits that were soluble when co-expressed in *E. coli* (refer Section 1.3.3) are positioned at two opposite poles on the  $\alpha$  ring. It would be worthwhile to investigate whether  $\alpha_3$  and  $\alpha_4$  could exhibit behavior akin to  $\alpha_7$  and  $\alpha_1$  and form HMWCs, and if so, whether they have an ability to incorporate their native neighbors.

The second aim of this project was to test, in vivo, for the presence of any HMWC complexes formed by  $\alpha_5$ ,  $\alpha_6$ ,  $\alpha_7$  and  $\alpha_1$  as these could be putative  $\alpha$  ring assembly intermediates or dead-end complexes whose formation must be avoided to

ensure efficient assembly. Interestingly, the HMWC seen with  $\alpha 5$ ,  $\alpha 6$ ,  $\alpha 7$  and  $\alpha 1$  is not observed in the presence of the assembly factor Pba3-Pba4 when these six proteins are co-expressed in *E. coli* (Chew and Kusmierczyk, unpublished). Instead, Pba3-Pba4 forms a complex with  $\alpha 5$ ,  $\alpha 6$ , and  $\alpha 7$  that was previously observed (Kusmierczyk, 2008b). If Pba3-Pba4 is able to suppress the formation of such subunit complexes in vitro, then we may be able to detect the formation of a HMWC with  $\alpha 5$ ,  $\alpha 6$ ,  $\alpha 7$  and  $\alpha 1$  (or some other combination) when Pba3-Pba4 is deleted in vivo. We now know that we can detect HMWCs containing  $\alpha 7$  and  $\alpha 1$  in vitro via the  $\alpha 1$ - $\alpha 1$  crosslink that all such complexes share. This suggests that  $\alpha 1$ - $\alpha 1$  crosslinks could serve as potential trackers to detect such high molecular weight complexes, should they assemble in vivo.

We can use the crosslinking strategy to look for  $\alpha 1$ - $\alpha 1$  crosslinks in yeast cells in which the Pba3-Pba4 assembly factor has been deleted. To this end, we have created *scl1 $\Delta$ pba4 $\Delta$*  yeast strains. Since deletion of *SCL1* (the gene that codes for  $\alpha 1$ ) is lethal to yeast cells, wild type *SCL1* is made available on a covering plasmid in these cells. The next step involves creating *scl1 $\Delta$ pba4 $\Delta$*  yeast strains in which the only source of  $\alpha 1$ , on a covering plasmid, would be the  $\alpha 1$  with no internal cysteines and having only the cross-linkable cysteine in it. These strains will be used to look for the presence of  $\alpha 1$ - $\alpha 1$  crosslinks which will suggest the presence of these HMWCs. To demonstrate that these HMWCs are forming, one could then attempt to purify them by incorporating an epitope tag (such as Flag) onto  $\alpha 1$  and carrying out pull down experiments. Native PAGE could then be used to separate these HMWCs from fully assembled 20S proteasomes (which will also contain Flag-tagged  $\alpha 1$ ).

## REFERENCES

## REFERENCES

- Beck, F., Unverdorben, P., Bohn, S., Schweitzer, A., Pfeifer, G., Sakata, E., Nickell, S., Plitzko, J.M., Villa, E., Baumeister, W. and Förster, F. (2012) Near-atomic resolution structural model of the yeast 26S proteasome. *Proceedings of the National Academy of Sciences of the United States of America* 109: 14870-14875
- Benaroudj, N. and Goldberg, A. L. (2000) PAN, the proteasome-activating nucleotidase from archaeobacteria, is a protein-unfolding molecular chaperone. *Nature cell biology* 2: 833-839
- Chen, P. and Hochstrasser, M. (1995) Biogenesis, structure and function of the yeast 20S proteasome. *The EMBO Journal* 14: 2620-2630
- Fang, S. and Weissman, A.M. (2004) A field guide to ubiquitylation. *Cellular and Molecular Life Sciences* 61: 1546-1561
- Finley D. (2009) Recognition and processing of ubiquitin-protein conjugates by the proteasome. *Annual Review of Biochemistry* 78: 477-513
- Gerards, W.L., Enzlin, J., Haner, M., Hendriks, I.L., Aebi, U., Bloemendal, H. and Boelens, W. (1997) The human alpha-type proteasomal subunit HsC8 forms a double ringlike structure, but does not assemble into proteasome-like particles with the beta-type subunits HsDelta or HsBPROS26. *The Journal of Biological Chemistry* 272: 10080-10086

- Gerards, W.L., de Jong, W.W., Bloemendal, H. and Boelens, W. (1998) The human proteasomal subunit HsC8 induces ring formation of other alpha-type subunits. *Journal of Molecular Biology* 275: 113-121
- Gillette T.G., Kumar, B., Thompson, D., Slaughter, C.A. and DeMartino, G.N. (2008) Differential roles of the COOH termini of AAA subunits of PA700 (19 S regulator) in asymmetric assembly and activation of the 26 S proteasome. *The Journal of Biological Chemistry* 283: 31813-31822
- Glickman, M.H., Rubin, D.M., Fried, V.A. and Finley, D. (1998) The Regulatory Particle of the *Saccharomyces cerevisiae* proteasome. *Molecular and Cellular Biology* 18: 3149-3162
- Groll, M., Ditzel, L., Löwe, J., Stock, D., Bochtler, M., Bartunik, H.D. and Huber R. (1997) Structure of 20S proteasome from yeast at 2.4 Å resolution. *Nature* 386: 463-71
- Hirano, Y., Hendil, K.B., Yashiroda, H., Iemura, S., Nagane, R., Hioki, Y., Natsume, T., Tanaka, K. and Murata, S. (2005) A heterodimeric complex that promotes the assembly of mammalian 20S proteasomes. *Nature* 437: 1381-1385
- Hirano, Y., Kaneko, T., Okamoto, K., Bai, M., Yashiroda, H., Furuyama, K., Kato, K., Tanaka, K. and Murata, S. (2008) Dissecting beta-ring assembly pathway of the mammalian 20S proteasome. *The EMBO Journal* 27: 2204-13
- Hwang, J., Winkler, L. and Kalejta, R.F. (2011) Ubiquitin-independent proteasomal degradation during oncogenic viral infections. *Biochimica et Biophysica Acta - Reviews on Cancer* 1816: 147-157
- Kunjappu, M.J. and Hochstrasser, M. (2014) Assembly of the 20S proteasome. *Biochimica et Biophysica Acta (BBA) - Molecular Cell Research* 1843: 2-12
- a. Kusmierczyk, A.R. and Hochstrasser, M. (2008) Some assembly required: dedicated chaperones in eukaryotic proteasome biogenesis. *Biological Chemistry* 389: 1143-115

- b. Kusmierczyk, A.R., Kunjappu, M.J., Funakoshi, M. and Hochstrasser, M. (2008) A multimeric assembly factor controls the formation of alternative 20S proteasomes. *Nature Structural and Molecular Biology* 15: 237-244
- Kusmierczyk, A.R., Kunjappu, M., Kim, R.Y. and Hochstrasser, M. (2011) A conserved 20S proteasome assembly factor requires a C-terminal HbYX motif for proteasomal precursor binding. *Nature Structural and Molecular Biology* 18: 622-629
- Lander, G.C., Estrin, E., Matyskiela, M.E., Bashore, C., Nogales, E. and Martin, A. (2012) Complete subunit architecture of the proteasome regulatory particle. *Nature* 482: 186-191
- Lowe, J., Stock, D., Jap, B., Zwickl, P., Baumeister, W. and Huber, R. (1995) Crystal structure of the 20S proteasome from the archaeon *T. acidophilum* at 3.4 Å resolution. *Science* 268: 533-539
- Li, X., Kusmierczyk, A., Wong, P., Emili, A. and Hochstrasser, M. (2007)  $\beta$ -Subunit appendages promote 20S proteasome assembly by overcoming an Ump1-dependent checkpoint. *The EMBO Journal* 26: 2339-2349
- Maupin-Furlow, J. (2011) Proteasomes and protein conjugation across domains of life. *Nature Reviews Microbiology* 10: 100-111
- Pouch, M-N., Cournoyer, B. and Baumeister, W. (2000) Characterization of the 20S proteasome from the actinomycete Frankia. *Molecular Microbiology* 35: 368-377
- Ramos P.C., Hoekendorff J., Johnson E.S., Varshavsky A. and Dohmen R.J. (1998) Ump1p is required for proper maturation of the 20S proteasome and becomes its substrate upon completion of the assembly. *Cell* 92: 489-499
- Stadtmueller, B.M., Kish-Trier, E., Ferrell, K., Petersen, C.N., Robinson, H., Myszka D.G, Eckert, D.M., Formosa, T. and Hill, C.P. (2012) Structure of a proteasome Pba1-Pba2 complex: implications for proteasome assembly, activation, and biological function. *The Journal of Biological Chemistry* 287: 37371-37382

- Sharon, M., Witt, S., Glasmacher, E., Baumeister, W. and Robinson C.V. (2007) Mass spectrometry reveals the missing links in the assembly pathway of the bacterial 20S proteasome. *The Journal of Biological Chemistry* 282: 18448-18457
- Smith, D.M., Chang, S-C., Park, S., Finley, D., Cheng, Y. and Goldberg, A.L. (2007) Docking of the proteasomal ATPases' carboxyl termini in the 20S proteasome's alpha ring opens the gate for substrate entry. *Molecular Cell* 27: 731-744
- Tamura, T., Nagy, I., Lupas, A., Lottspeich, F., Cejka, Z., Schoofs, G., Tanaka, K., Mot, R.D. and Baumeister, W. (1995) The first characterization of a eubacterial proteasome: the 20S complex of *Rhodococcus*. *Current Biology* 5: 766-774
- Velichutina, I., Connerly, P.L., Arendt, C.S., Li, X. and Hochstrasser, M. (2004) Plasticity in eucaryotic 20S proteasome ring assembly revealed by a subunit deletion in yeast. *The EMBO Journal* 23: 500-510
- Wilk, S. and Orłowski, M. (1983) Evidence that pituitary cation-sensitive neutral endopeptidase is a multicatalytic protease complex. *Journal of Neurochemistry* 40: 842-849
- Yao, Y., Toth, C.R., Huang, L., Wong, M.L., Dias, P., Burlingame, A.L., Coffino, P. and Wang, C.C. (1999) alpha5 subunit in *Trypanosoma brucei* proteasome can self-assemble to form a cylinder of four stacked heptamer rings. *Biochemical Journal* 344: 349-358
- Zwickl, P., Kleinz, J. and Baumeister W. (1994) Critical elements in proteasome assembly. *Nature Structural & Molecular Biology* 1: 765-770
- Zwickl, P., Ng, D., Woo, K. M., Klenk, H. P. and Goldberg, A. L. (1999) An archaeobacterial ATPase, homologous to ATPases in the eukaryotic 26 S proteasome, activates protein breakdown by 20 S proteasomes. *The Journal of Biological Chemistry* 274: 26008-26014

## TABLES

Table 1. Proteasome and protein conjugation system across the domains of life (Modified and reproduced from Maupin-Furlow, 2011).

Domain	Bacteria	Archaea	Eukarya
Protein Conjugation System	Pupylation	Sampylation	Ubiquitination
Types of 20S subunits	One/two different types of $\alpha$ and $\beta$	One/two different types of $\alpha$ and $\beta$	Seven different types of $\alpha$ ( $\alpha$ 1-7) and $\beta$ ( $\beta$ 1-7)
AAA-ATPase regulators of 20S proteasome	AAA+ ATPase forming a Ring-shaped Complex (Arc)	Proteasome-Activating Nucleotidases (PAN)	19S Regulatory Particle (RP)

Table 2. Plasmids used in this study.

Name	Description	Organism
AKB80	pET11a $\alpha 5$ , $\alpha 6$ , $\alpha 7$ , $\alpha 1$ -His	<i>S. cerevisiae</i>
AKB143	pET11a $\alpha 7$ , $\alpha 1$ -His	<i>S. cerevisiae</i>
AKB145	pET11a $\alpha 6$ , $\alpha 7$ , $\alpha 1$ -His	<i>S. cerevisiae</i>
AKB191	pET42 $\alpha$ -His	<i>M. maripaludis</i>
AKB600	pET42 $\alpha$ (Q99C)-His	<i>M. maripaludis</i>
AKB706	pET42 $\alpha$ (A98C)-His	<i>M. maripaludis</i>
AKB707	pET42 $\alpha$ (M100C)-His	<i>M. maripaludis</i>
AKB708	pET42 $\alpha$ (no cysteines)-His	<i>M. maripaludis</i>
AKB709	pET42 $\alpha$ (Q99C, no internal cysteines)-His	<i>M. maripaludis</i>
AKB752	pET11a $\alpha 5$ , $\alpha 6$ , $\alpha 7$ (A97C), $\alpha 1$ -His	<i>S. cerevisiae</i>
AKB753	pET11a $\alpha 5$ , $\alpha 6$ , $\alpha 7$ , $\alpha 1$ (A102C)-His	<i>S. cerevisiae</i>
AKB754	pET11a $\alpha 5$ , $\alpha 6$ , $\alpha 7$ (A97C), $\alpha 1$ (A102C)-His	<i>S. cerevisiae</i>
AKB780	prset5 $\alpha$ -His	<i>T. acidophilum</i>
AKB785	pET11a $\alpha 5$ , $\alpha 6$ , $\alpha 7$ (no cysteines), $\alpha 1$ -His	<i>S. cerevisiae</i>
AKB786	pET11a $\alpha 5$ , $\alpha 6$ , $\alpha 7$ (A97C, no internal cysteines), $\alpha 1$ -His	<i>S. cerevisiae</i>
AKB787	pET11a $\alpha 5$ , $\alpha 6$ , $\alpha 7$ , $\alpha 1$ (no cysteines)-His	<i>S. cerevisiae</i>
AKB788	pET11a $\alpha 5$ , $\alpha 6$ , $\alpha 7$ , $\alpha 1$ (A102C, no internal cysteines)-His	<i>S. cerevisiae</i>
AKB789	pET11a $\alpha 5$ , $\alpha 6$ , $\alpha 7$ (A97C, no internal cysteines), $\alpha 1$ (A102C, no internal cysteines)-His	<i>S. cerevisiae</i>
AKB796	pET11a $\alpha 5$ , $\alpha 6$ , $\alpha 7$ (no cysteines), $\alpha 1$ (no cysteines)-His	<i>S. cerevisiae</i>
AKB883	pET11a $\alpha 7$ , $\alpha 1$ (A102C, no internal cysteines)-His	<i>S. cerevisiae</i>
AKB885	pET11a $\alpha 6$ , $\alpha 7$ , $\alpha 1$ (A102C, no internal cysteines)-His	<i>S. cerevisiae</i>

## FIGURES

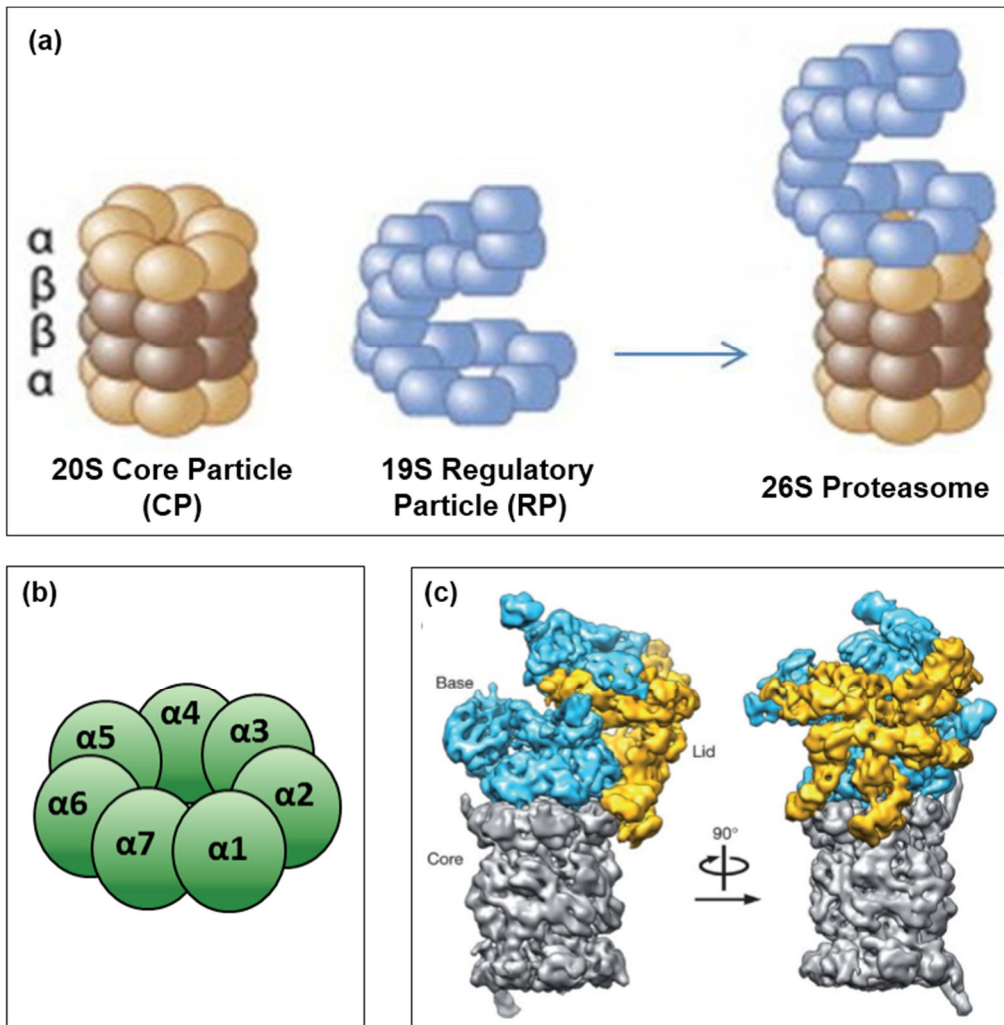


Figure 1. Structure of the proteasome. (a) Representation of the 20S CP, 19S RP and 26S Proteasome (Hwang et al., 2011). (b) Representation of positions of *S. cerevisiae*  $\alpha$  subunits relative to each other in  $\alpha$  ring of 20S proteasome. (c) Negative-stain three-dimensional reconstruction of the proteasome holoenzyme at approximately 15 Å resolution. Locations of 19S RP lid are in yellow and 19S RP base in cyan (Lander et al., 2012).

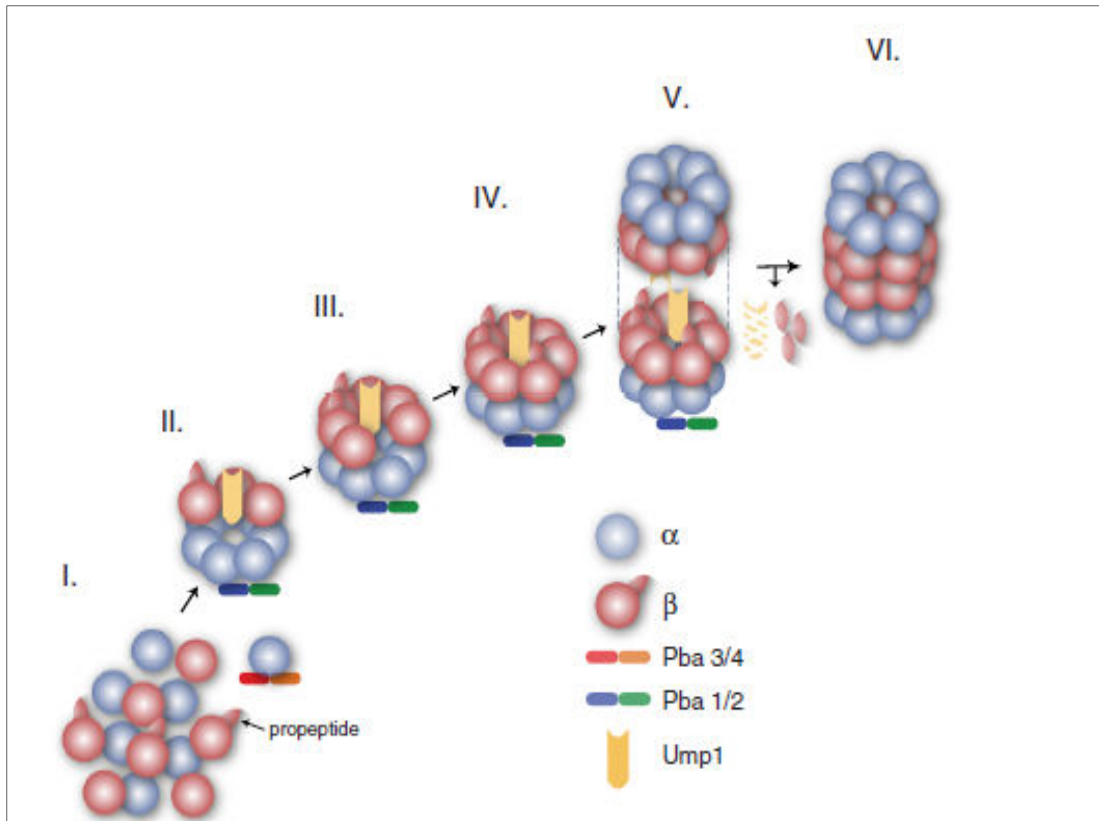


Figure 2. Model for assembly of 20S CP in yeast (Kunjappu and Hockstasser, 2014).

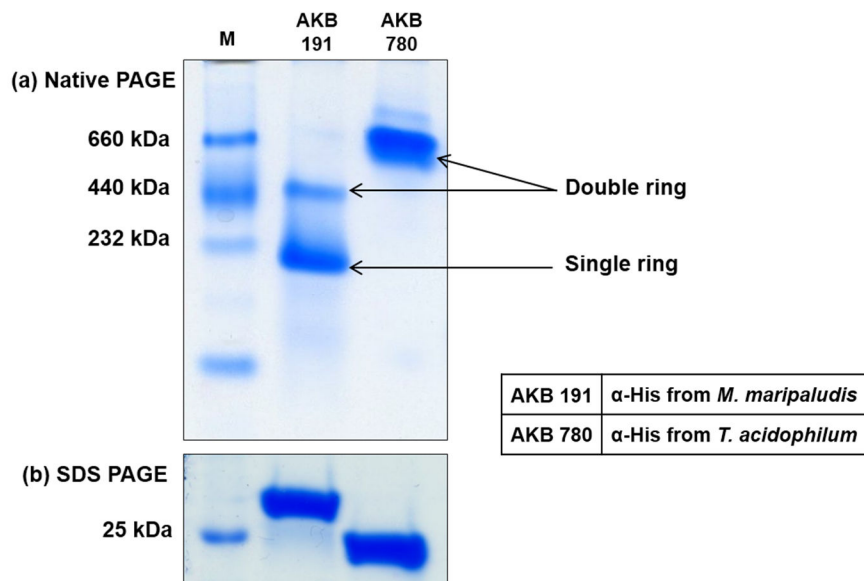


Figure 3. Archaeal  $\alpha$  subunits form double rings. (a) Eluates of *E. coli* expressing  $\alpha$  subunits from *M. maripaludis* (AKB191) and *T. acidophilum* (AKB780) were affinity purified by IMAC and electrophoresed on non-denaturing 4-15% gradient gel. (b) Purified eluates of AKB191 and AKB780, reduced with 600 mM DTT and electrophoresed on 10% denaturing gel. 10  $\mu$ g of purified protein was loaded in each lane, and the gels were stained with GelCode blue. M– Size standards.

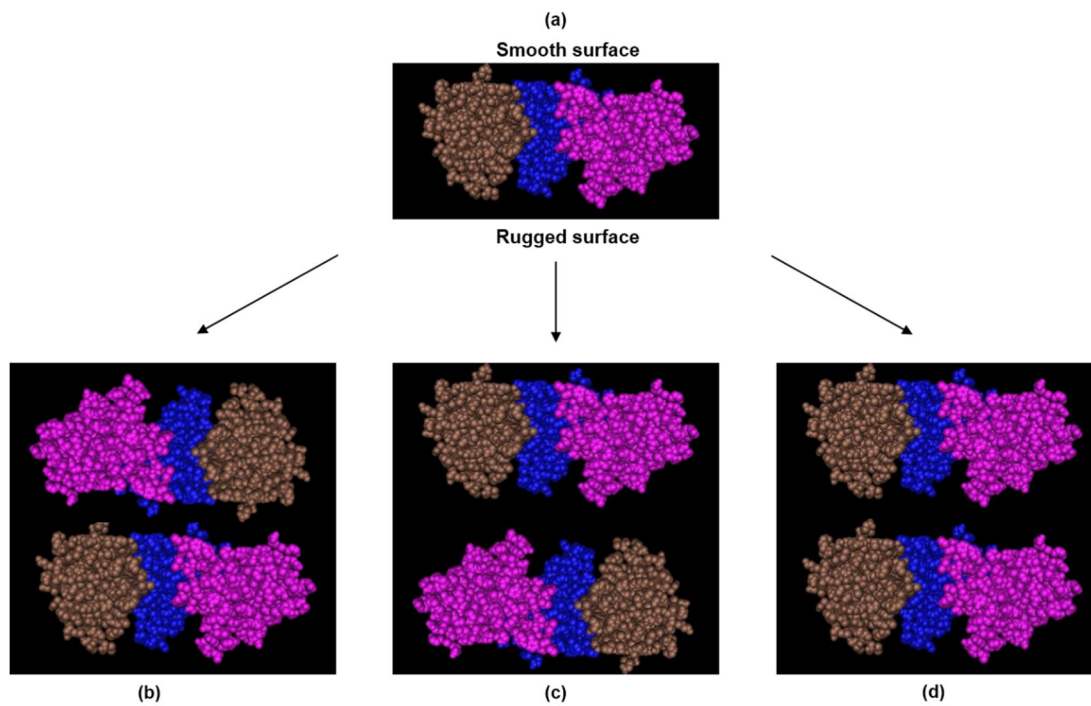


Figure 4.  $\alpha$  subunits of *T. acidophilum*. (a) Cn3D image of three out seven  $\alpha$  subunits as present in the heptameric  $\alpha$  ring in a 20S proteasome; view as seen from inside the 20S core, towards the outside. Also shown are theoretically predicted outcomes for double  $\alpha$  ring interactions wherein the two smooth surfaces are in close proximity (b), two rugged surfaces are in close proximity (c), and a rugged and smooth surface are in close proximity (d).

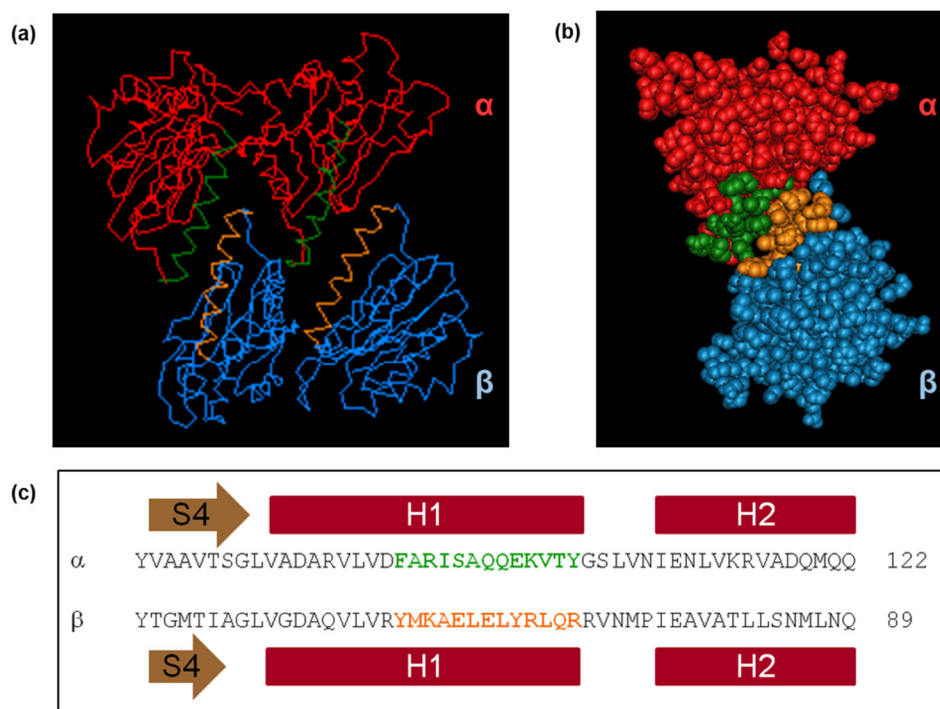


Figure 5. Subunit contacts between an  $\alpha$  (red) and  $\beta$  (blue) subunit, viewed from inside the 20S cavity. (a) Protein backbones of two  $\alpha$  and  $\beta$  subunits from *T. acidophilum* are shown, helices H1 are indicated in green and orange (b) A pair of  $\alpha$  and  $\beta$  subunits (protein backbone with side chains) are represented, the C-terminal halves of H1 helices are indicated in green and orange (c) The C-terminal halves of H1 helices are also indicated in green and orange in the sequence alignment of  $\alpha$  and  $\beta$  subunits (Figure reproduced and modified from data by Kusmierczyk, unpublished).

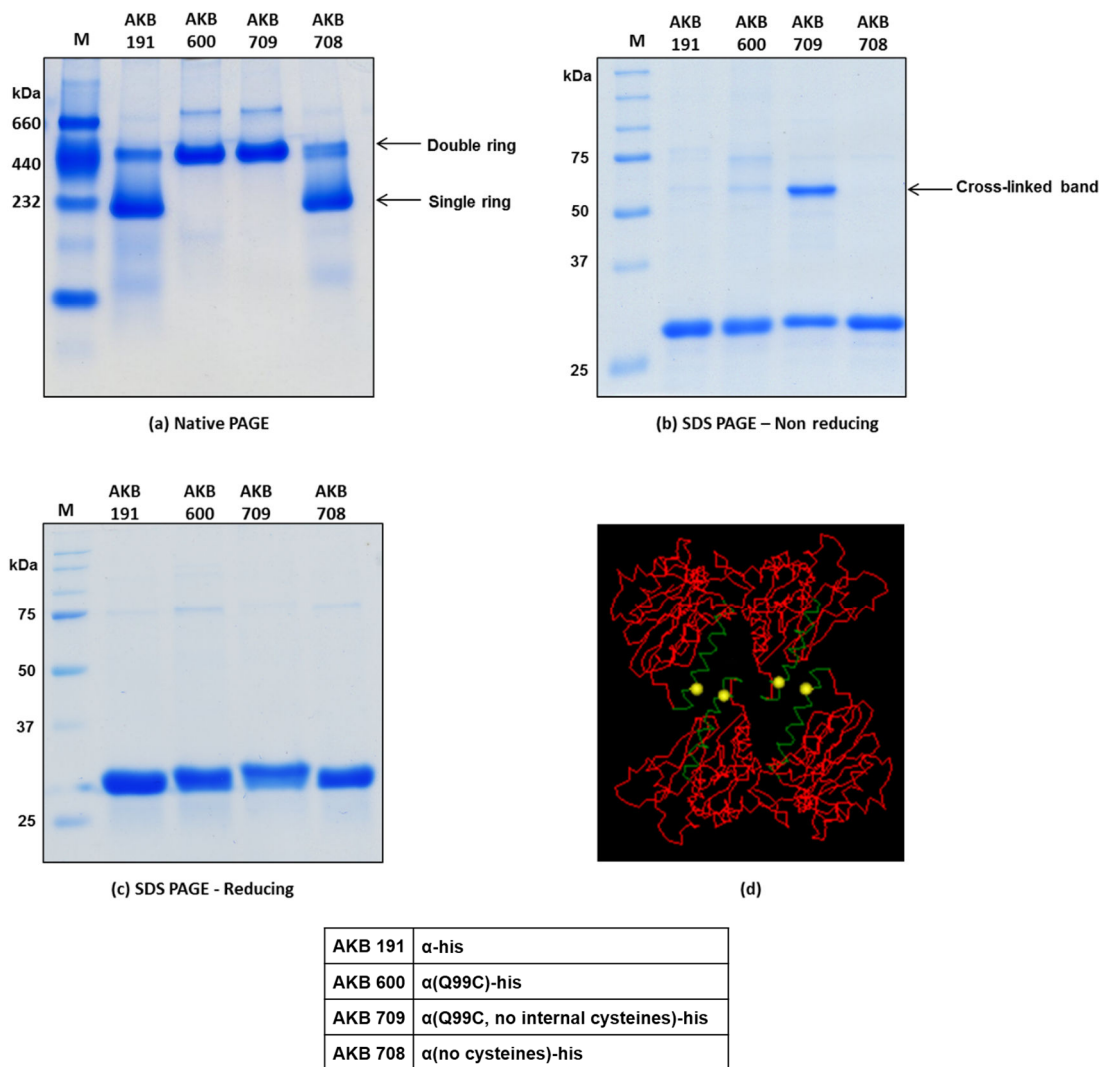


Figure 6. Efficient double ring formation in the presence of a cross-linkable cysteine in archaeal  $\alpha$  subunit. (a) Eluates of *E. coli* expressing wild type  $\alpha$  subunits (AKB191), Q99C mutant (AKB600), Q99C mutant with no internal cysteines (AKB709) and  $\alpha$  subunits with no cysteines (AKB708) from *M. maripaludis* were affinity purified by IMAC and electrophoresed on non-denaturing 4-15% gradient gel. (b) Purified eluates of AKB191, AKB600, AKB709 and AKB708 were electrophoresed on 10% denaturing gel under non-reducing conditions. (c) Purified eluates of AKB191, AKB600, AKB709 and AKB708 were reduced with 600 mM DTT and electrophoresed on 10% denaturing gel. 10  $\mu$ g of purified protein was loaded in each lane, and the gels were stained with GelCode blue. M– Size standards. (d) A proposed representation of double  $\alpha$  rings of *T. acidophilum*, showing two  $\alpha$  subunits of each ring (red) with their H1 helices (green). Amino acids corresponding to *M. maripaludis*  $\alpha$  subunit Q99C are indicated in yellow.

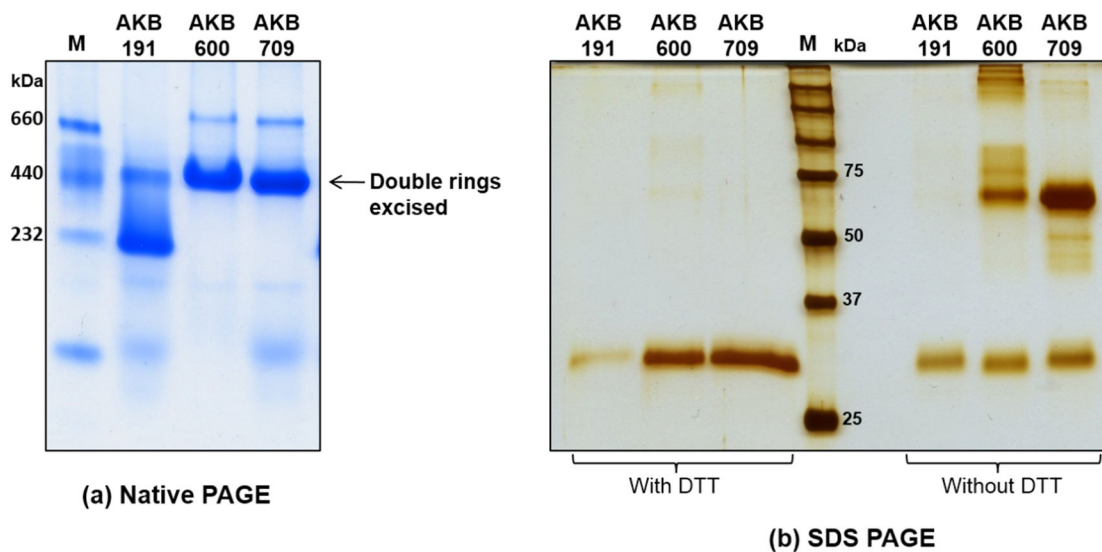


Figure 7. Presence of cross-linked  $\alpha$ - $\alpha$  dimer bands in archaeal double rings. (a) Eluates of *E. coli* expressing wild type  $\alpha$  subunits (AKB191), Q99C mutant (AKB600), Q99C mutant with no internal cysteines (AKB709) and  $\alpha$  subunits with no cysteines (AKB708) from *M. maripaludis* were affinity purified by IMAC and electrophoresed on non-denaturing 4-15% gradient gel. (b) The double rings indicated were excised and proteins thus eluted were mixed with Laemmli without DTT; aliquots of these eluates were mixed with 5xLaemmli and 600 mM DTT. These eluates were electrophoresed on 12 % denaturing gel and visualized by silver staining.

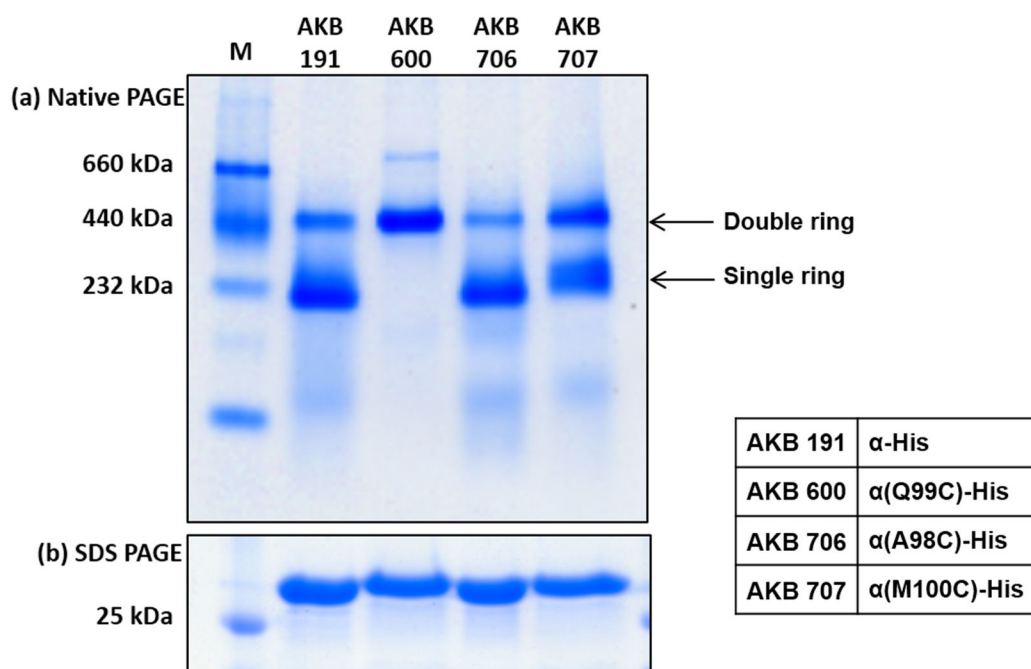


Figure 8. Efficient double ring formation depends on the position of the introduced cross-linkable cysteine. (a) Eluates of *E. coli* expressing wild type  $\alpha$  subunits (AKB191), Q99C mutant (AKB600), A98C mutant (AKB706) and M100C mutant (AKB707) from *M. maripaludis* were affinity purified by IMAC and electrophoresed on non-denaturing 4-15% gradient gel. (b) Purified eluates of AKB191, AKB600, AKB706 and AKB707, reduced with 600 mM DTT and electrophoresed on 10% denaturing gel. 10  $\mu$ g of purified protein was loaded in each lane, and the gels were stained with GelCode blue. M– Size standards.

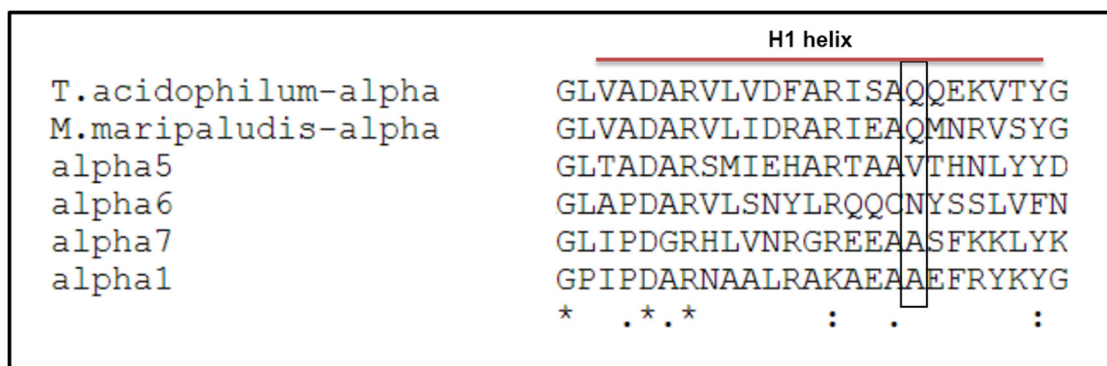


Figure 9. ClustalW alignment of  $\alpha$  subunits from *T. acidophilum*, *M. maripaludis*, and  $\alpha 5$ ,  $\alpha 6$ ,  $\alpha 7$ ,  $\alpha 1$  from *S. cerevisiae*. Residues that correspond to Q99 of *M. maripaludis*  $\alpha$  subunit are encased in the sequence alignment.

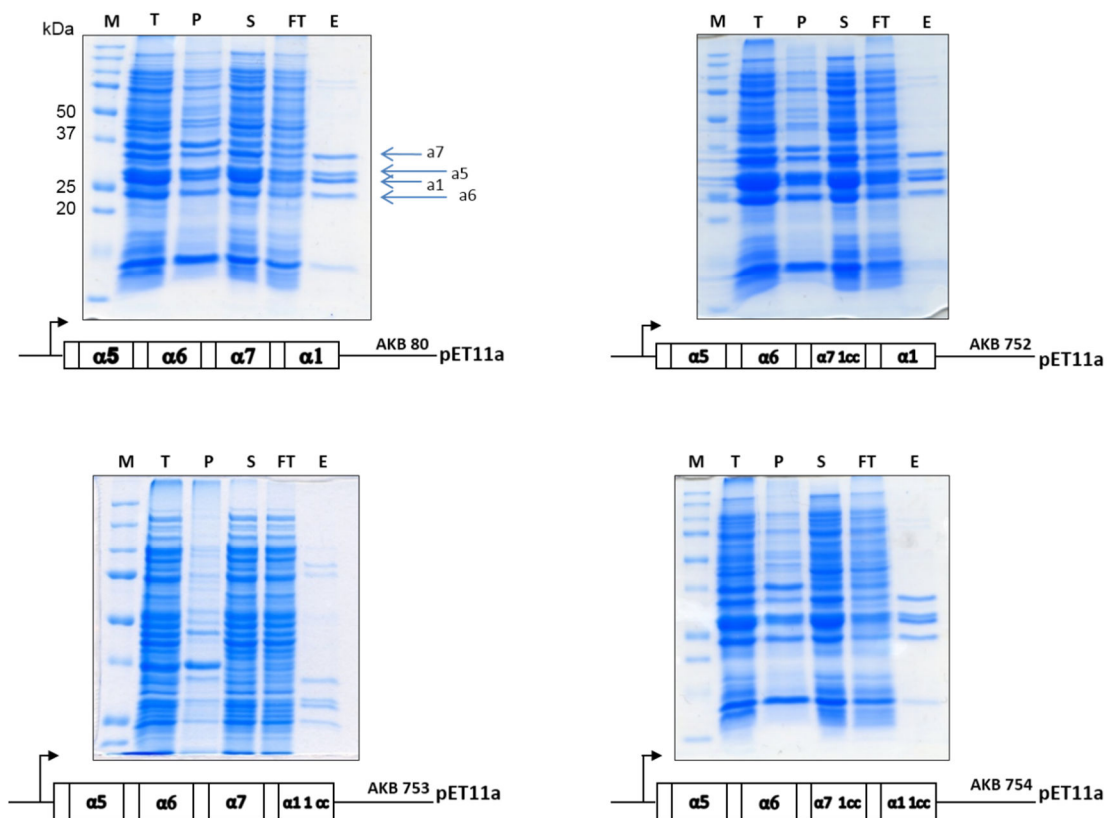
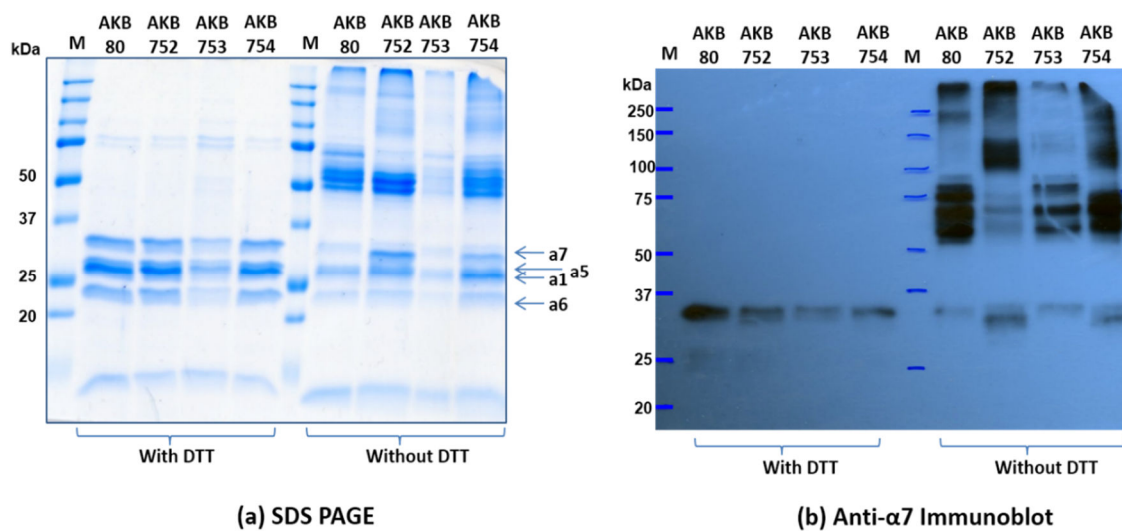
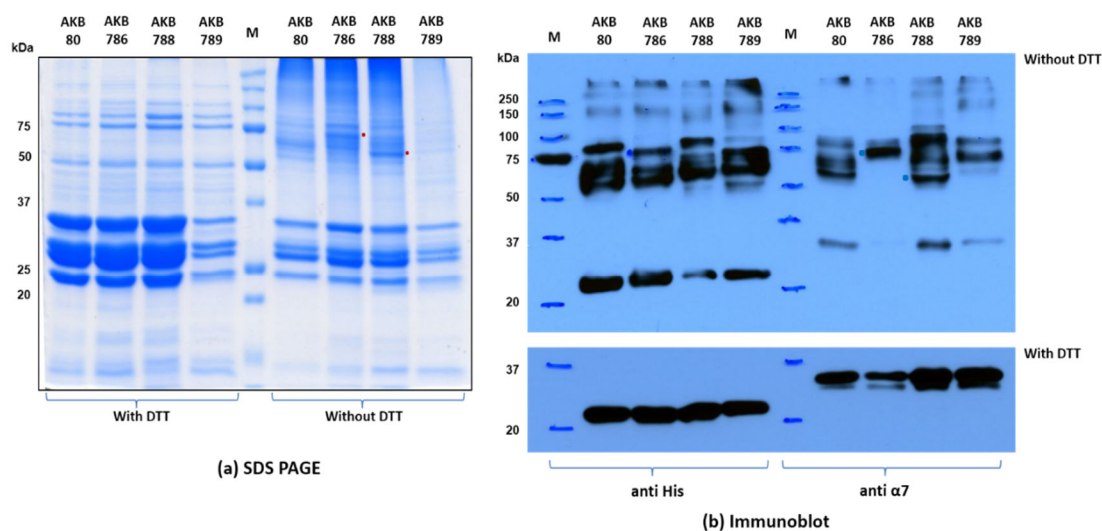


Figure 10. Expression profiling of AKB80 mutants. AKB80, AKB752, AKB753 and AKB754 were expressed in *E. coli*. Total (T), pellet (P), soluble (S), flow through (FT) and purified eluate (E) fractions of these constructs electrophoresed on 12% denaturing gel, stained with GelCode blue. 1cc- presence of cross-linkable cysteine, M- Size standards.



AKB 80	$\alpha$ 5 $\alpha$ 6 $\alpha$ 7 $\alpha$ 1-his
AKB 752	$\alpha$ 5 $\alpha$ 6 $\alpha$ 7(A97C) $\alpha$ 1-his
AKB 753	$\alpha$ 5 $\alpha$ 6 $\alpha$ 7 $\alpha$ 1(A102C)-his
AKB 754	$\alpha$ 5 $\alpha$ 6 $\alpha$ 7(A97C) $\alpha$ 1(A102C)-his

Figure 11. Detection of cross-linked bands in AKB80 mutants with cross-linkable cysteine. Eluates of *E. coli* expressing  $\alpha$  subunits from AKB80, AKB752, AKB753 and AKB754 were affinity purified by IMAC. (a) Purified eluates were electrophoresed on 10% denaturing gel under reducing and non-reducing conditions. The gel was stained with GelCode blue. (b) Western blot analysis with MCP72 probe that detects  $\alpha$ 7 of purified eluates of AKB80, AKB752, AKB753 and AKB754, cross-linked in the presence of 0.2 mM  $\text{CuCl}_2$ , with or without DTT. M – size standards.



AKB 80	$\alpha 5\alpha 6\alpha 7\alpha 1$ -his
AKB 786	$\alpha 5\alpha 6\alpha 7$ (A97C, no internal cysteines) $\alpha 1$ -his
AKB 788	$\alpha 5\alpha 6\alpha 7\alpha 1$ (A102C, no internal cysteines)-his
AKB 789	$\alpha 5\alpha 6\alpha 7$ (A97C, no internal cysteines) $\alpha 1$ (A102C, no internal cysteines)-his

Figure 12. Detection of cross-linked bands in AKB80 mutants with cross-linkable cysteine but no internal cysteines. Eluates of *E. coli* expressing  $\alpha$  subunits from AKB80, AKB786, AKB788 and AKB789 were affinity purified by IMAC. (a) Purified eluates were electrophoresed on 10% denaturing gel under reducing and non-reducing conditions. The gel was stained with GelCode blue. (b) Western blot analysis with MCP72 probe (that detects  $\alpha 7$ ), and anti-his antibodies (that detect  $\alpha 1$ ) of purified eluates of AKB80, AKB786, AKB788 and AKB789, cross-linked in the presence of 0.2 mM  $\text{CuCl}_2$ , with or without DTT. M – size standards.

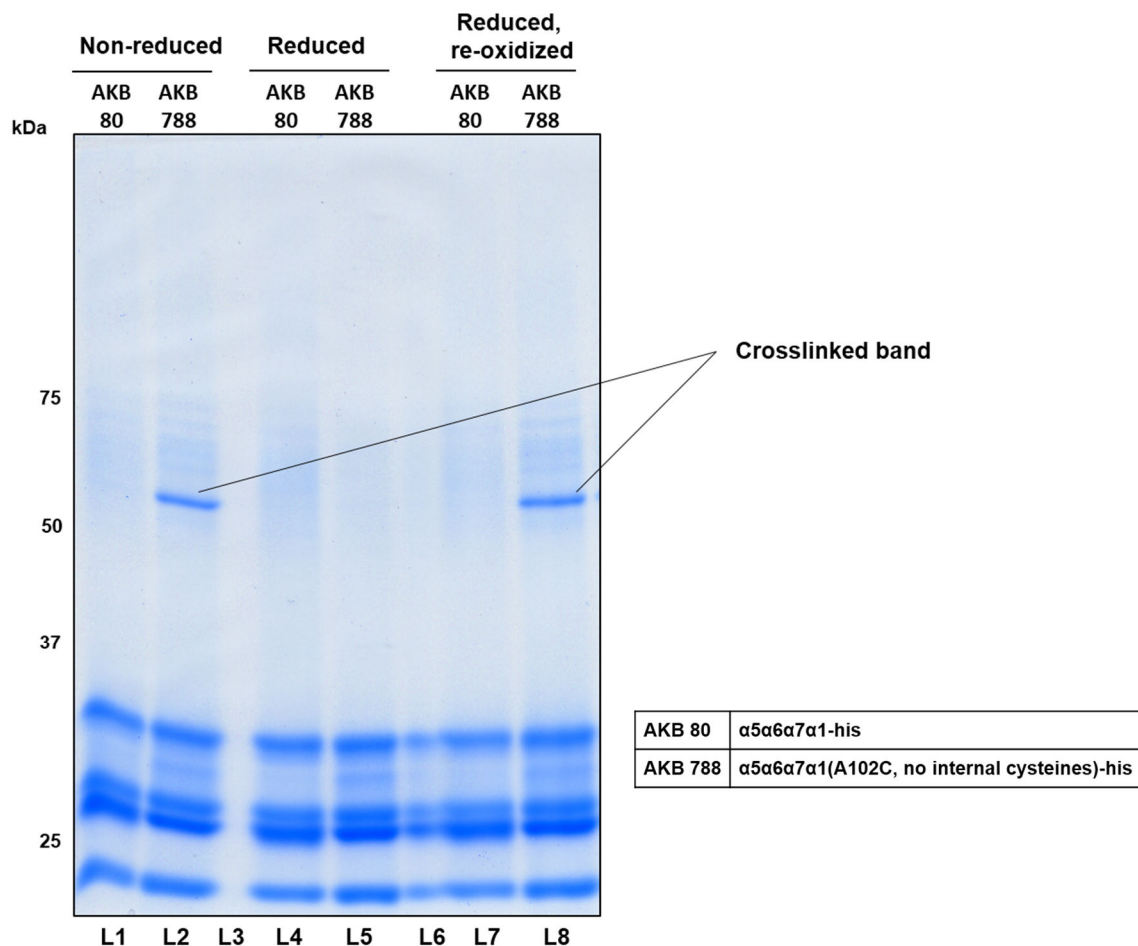


Figure 13. Crosslinking analysis of AKB80 and its mutant with cross-linkable cysteine in  $\alpha 1$ . AKB80 ( $\alpha 5\alpha 6\alpha 7\alpha 1$ -his) and AKB788 ( $\alpha 5\alpha 6\alpha 7\alpha 1$ (A102C, no internal cysteines)-his) were expressed in *E. coli* and affinity purified by IMAC. Purified eluates of 20  $\mu\text{g}$  were electrophoresed on a 10% denaturing gel under non-reducing conditions along with a second set of purified eluates of 20  $\mu\text{g}$  that were reduced with 1 mM DTT. A third set of purified eluates reduced with 1 mM DTT was passed through PD 25 columns to eliminate DTT, the resulting eluate was applied to TALON-resin charged with cobalt to facilitate oxidation, 20  $\mu\text{g}$  of these eluates were also electrophoresed along with the above mentioned proteins. The 10% denaturing gel was stained with GelCode Blue.

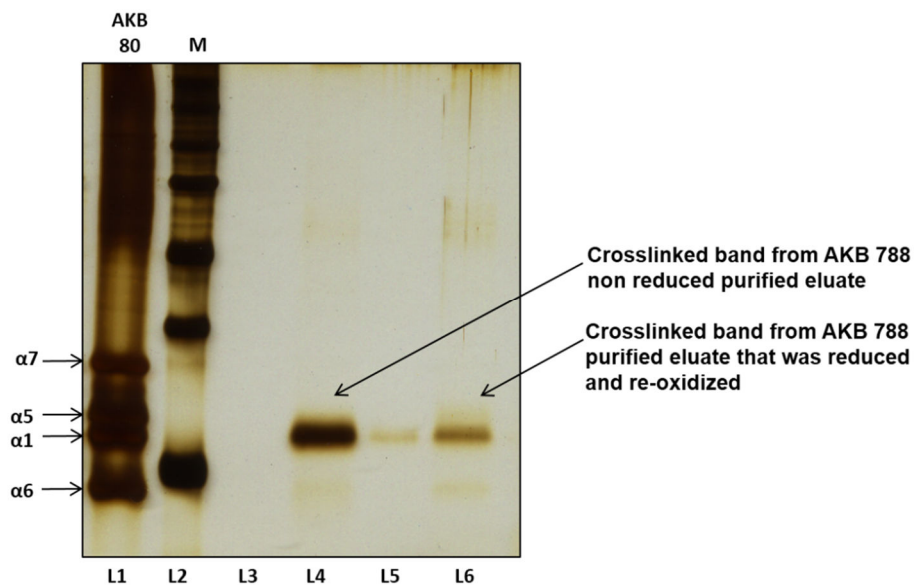


Figure 14. Reduction of cross-linked bands from AKB788. As indicated in Figure 12, the cross-linked band that appeared in the non-reduced purified eluate of AKB788, and the cross-linked band that appeared upon re-oxidation after reduction of the purified eluate, were excised and the proteins thus eluted were reduced with 600 mM DTT and electrophoresed on a 12% denaturing gel. The gel was visualized by silver staining. M-Size standards.

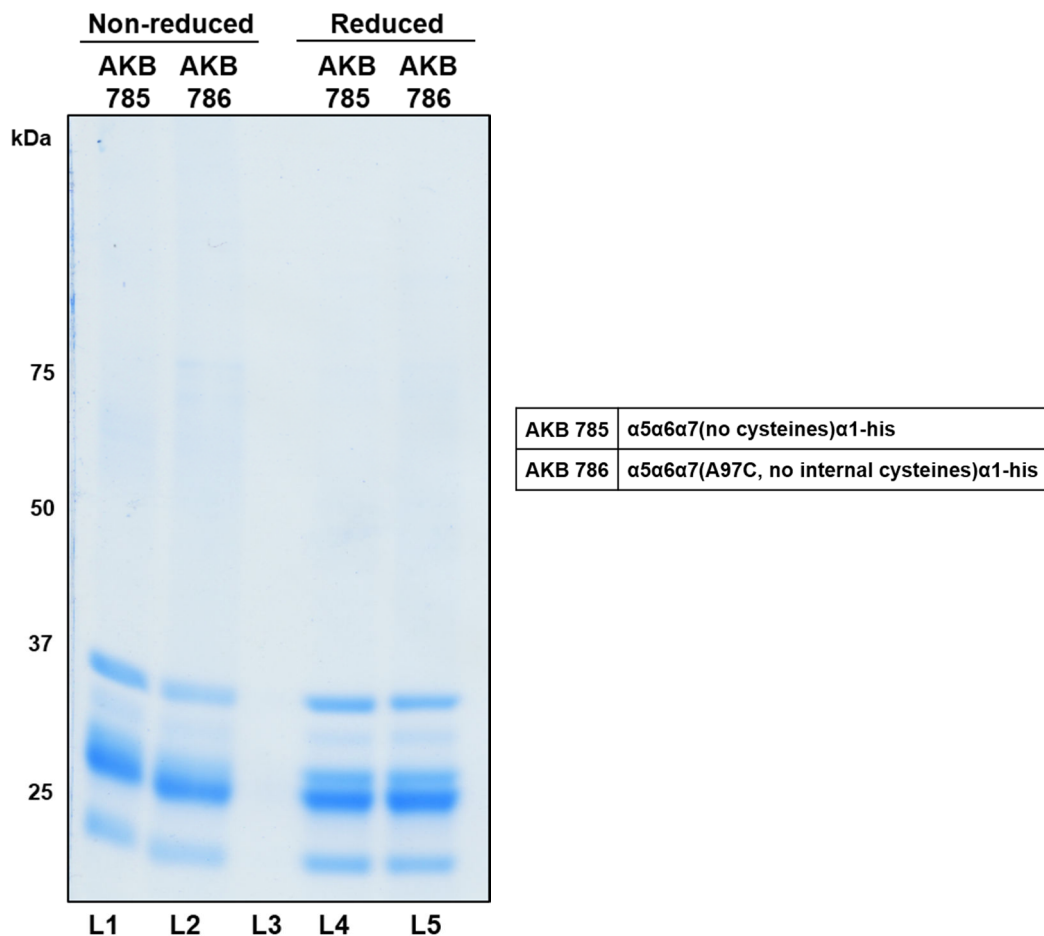


Figure 15. Crosslinking analysis of an AKB80 mutant with cross-linkable cysteine in  $\alpha 7$ . AKB786 ( $\alpha 5\alpha 6\alpha 7(\text{A97C, no internal cysteines})\alpha 1\text{-his}$ ) and its control AKB785 ( $\alpha 5\alpha 6\alpha 7(\text{no cysteines})\alpha 1\text{-his}$ ) were expressed in *E. coli* and affinity purified by IMAC. Purified eluates of 20  $\mu\text{g}$  were electrophoresed on a 10% denaturing gel under non-reducing conditions along with a second set of purified eluates of 20  $\mu\text{g}$  that were reduced with 1 mM DTT. The 10% denaturing gel was stained with GelCode Blue.

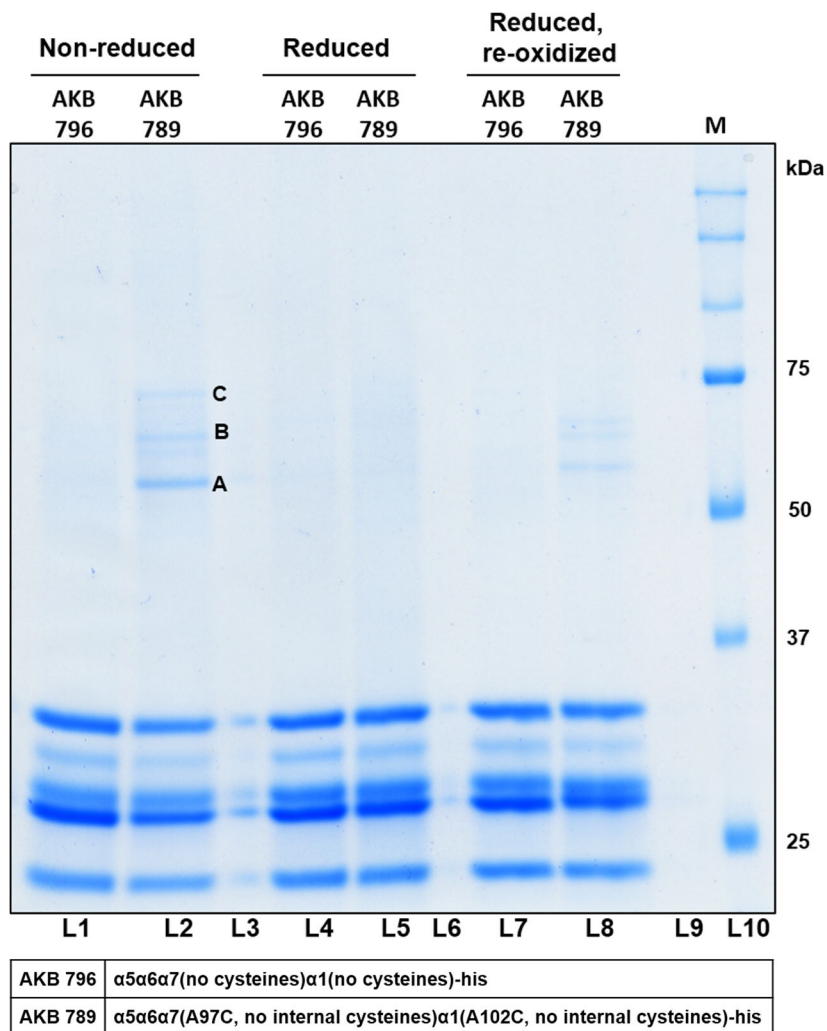


Figure 16. Crosslinking analysis of an AKB80 mutant with cross-linkable cysteine in  $\alpha 7$  and  $\alpha 1$ . AKB789 ( $\alpha 5\alpha 6\alpha 7$ (A97C, no internal cysteines) $\alpha 1$ (A102C, no internal cysteines)-his) and its control AKB796 ( $\alpha 5\alpha 6\alpha 7$ (no cysteines) $\alpha 1$ (no cysteines)-his) were expressed in *E. coli* and affinity purified by IMAC. Purified eluates of 20  $\mu$ g were electrophoresed on a 10% denaturing gel under non-reducing conditions along with a second set of purified eluates of 20  $\mu$ g that were reduced with 1 mM DTT, and a third set of purified eluates of 20  $\mu$ g reduced with 1 mM DTT and re-oxidized in the presence of 50  $\mu$ M  $\text{CuCl}_2$ . Cross-linked bands present in the purified eluates under non-reducing conditions are indicated. The 10% denaturing gel was stained with GelCode Blue. M- Size standards.

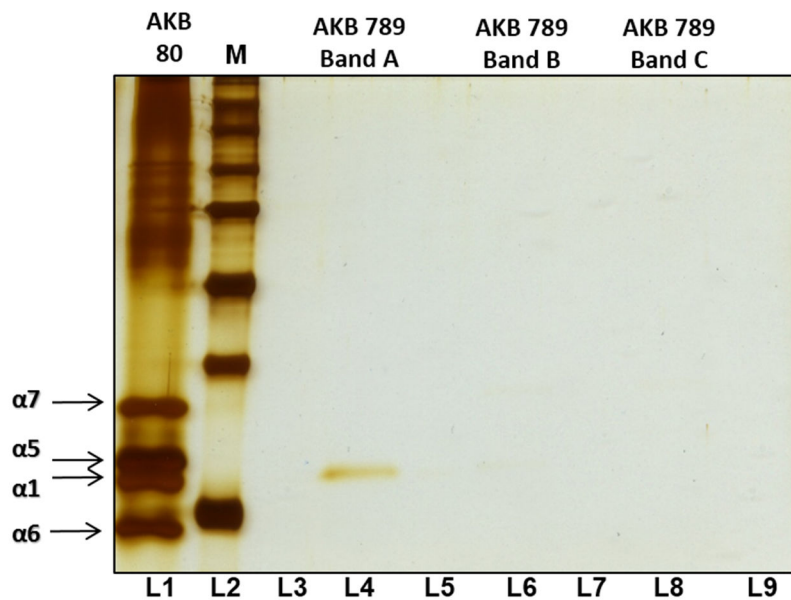


Figure 17. Reduction of cross-linked bands from AKB789. As indicated in Figure 15, the cross-linked bands that appeared in the purified eluates under non-reducing conditions were excised and the proteins thus eluted were reduced with 600 mM DTT and electrophoresed on a 12% denaturing gel. The gel was visualized by silver staining. M-Size standards.

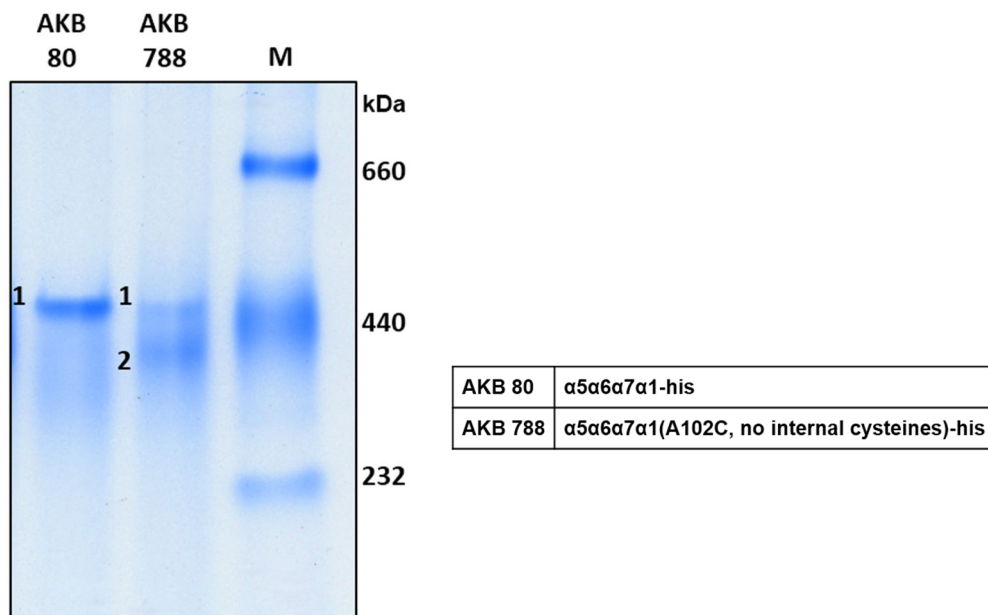


Figure 18. High molecular weight complexes in AKB80 and AKB788.  $\alpha$  subunits of AKB80 and AKB788 expressed in *E. coli* were affinity purified by IMAC and electrophoresed on 5% non-denaturing gel. High molecular weight complexes formed are numbered in individual lanes. M- Size standards.

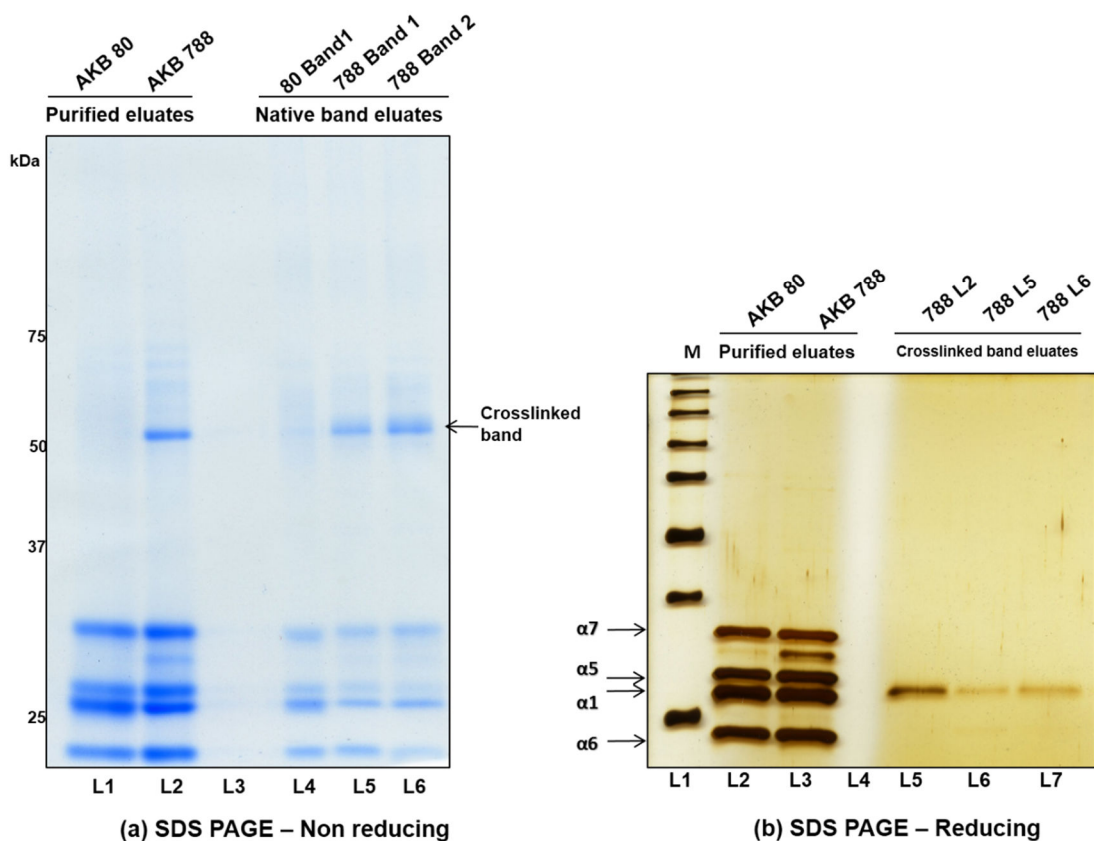


Figure 19. Crosslinking analysis of high molecular weight complexes (HMWCs) formed by AKB788. (a) HMWCs of AKB80 and AKB788 shown in Figure R17 were excised from the gel and the proteins were eluted under non-reducing conditions. These eluates were electrophoresed on 10% denaturing gel, alongside non-reduced eluates of AKB80 and AKB788 originally affinity purified by IMAC. Cross-linked bands are indicated. (b) Proteins from the cross-linked bands were eluted, reduced with 600 mM DTT and electrophoresed on 12 % denaturing gel. The gel was visualized by silver staining. M-Size standards.

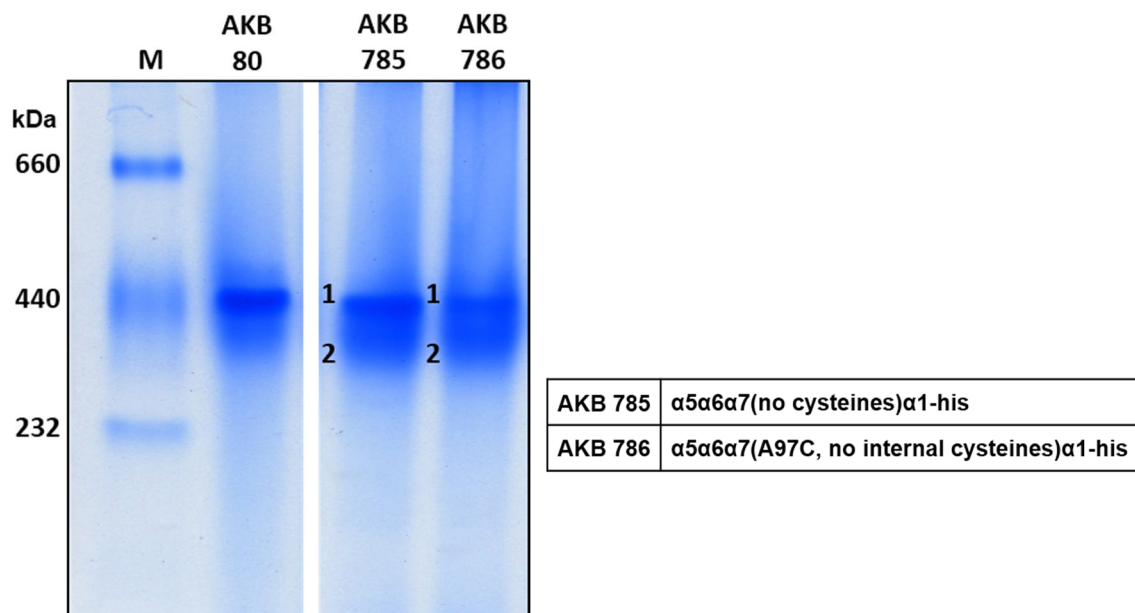


Figure 20. High molecular weight complexes in AKB785 and AKB786.  $\alpha$  subunits of AKB785 and AKB786 expressed in *E. coli* were affinity purified by IMAC and electrophoresed on 5% non-denaturing gel. High molecular weight complexes formed are numbered in individual lanes. M- Size standards.

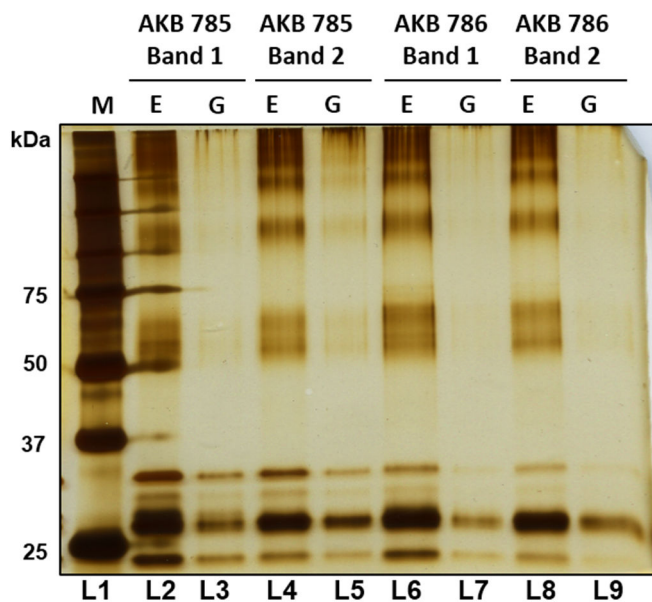


Figure 21. Crosslinking analysis of high molecular weight complexes (HMWCs) formed by AKB785 and AKB786. (a) HMWCs of AKB785 and AKB786 shown in Figure R20 were excised from the gel and the proteins were eluted under non-reducing conditions. These eluates were electrophoresed on 12% denaturing gel. The gel was visualized by silver staining. G – gel slices of excised bands, E – corresponding eluate fractions. M-Size standards.

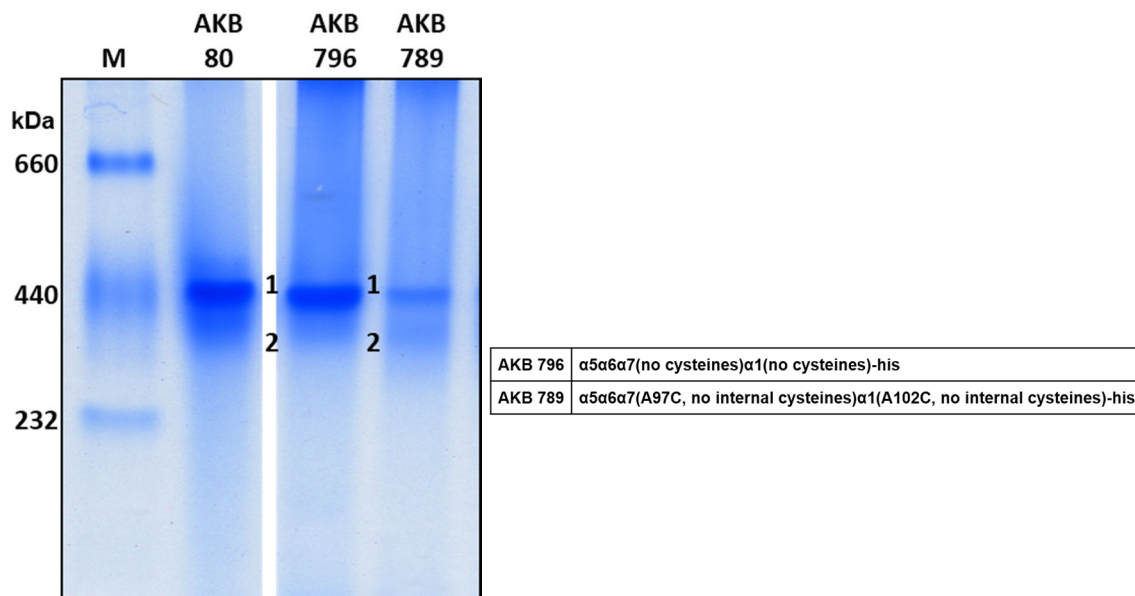


Figure 22. High molecular weight complexes in AKB796 and AKB789.  $\alpha$  subunits of AKB789 and AKB796 expressed in *E. coli* were affinity purified by IMAC and electrophoresed on 5% non-denaturing gel. High molecular weight complexes formed are numbered in individual lanes. M- Size standards.

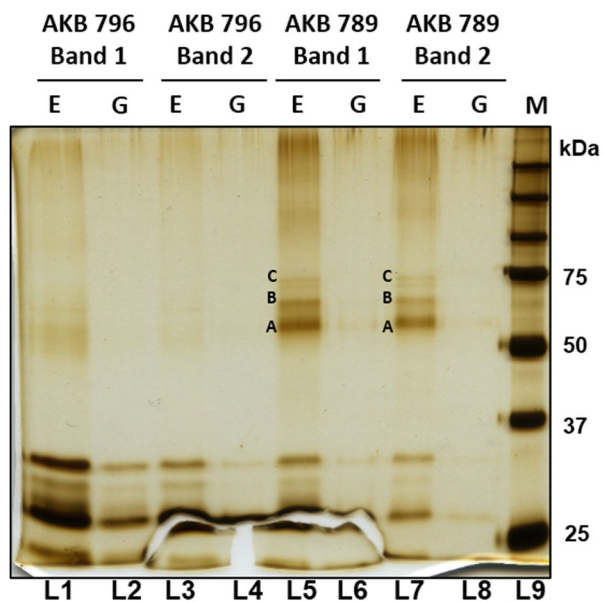


Figure 23. Crosslinking analysis of high molecular weight complexes (HMWCs) formed by AKB796 and AKB789. (a) HMWCs of AKB796 and AKB789 shown in Figure R22 were excised from the gel and the proteins were eluted under non-reducing conditions. These eluates were electrophoresed on 12% denaturing gel. The gel was visualized by silver staining. Cross-linked bands are indicated. G – gel slices of excised bands, E – corresponding eluate fractions. M- Size standards.

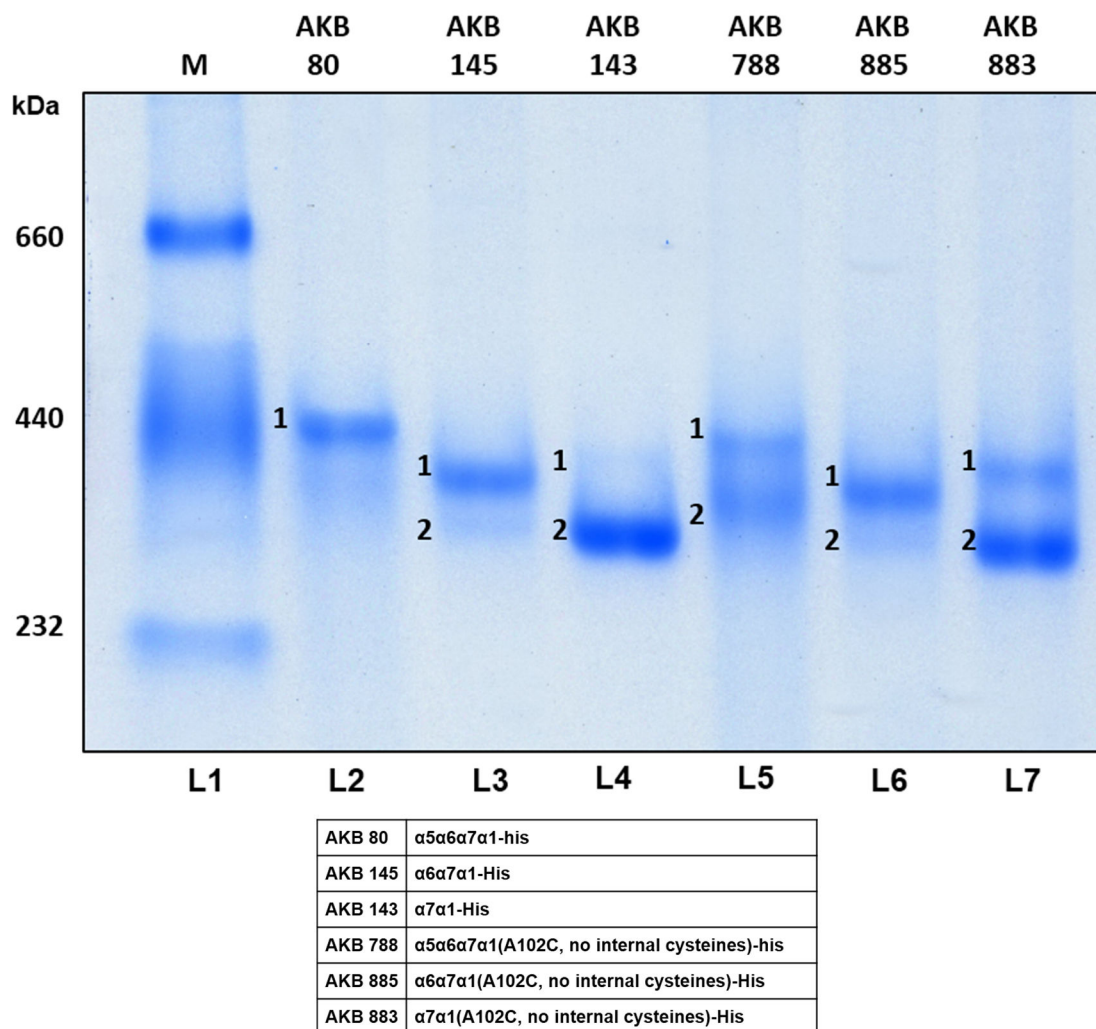


Figure 24. High molecular weight complexes formed when  $\alpha 5$ ,  $\alpha 6$ ,  $\alpha 7$  and  $\alpha 1$  are co-expressed in different combinations.  $\alpha$  subunits of AKB80, AKB145 and AKB143 and their mutants which contain a cross-linkable cysteine in  $\alpha 1$  namely AKB788, AKB885 and AKB883 respectively, expressed in *E. coli* were affinity purified by IMAC and electrophoresed on 5% non-denaturing gel. High molecular weight complexes formed are numbered in individual lanes. M- Size standards.

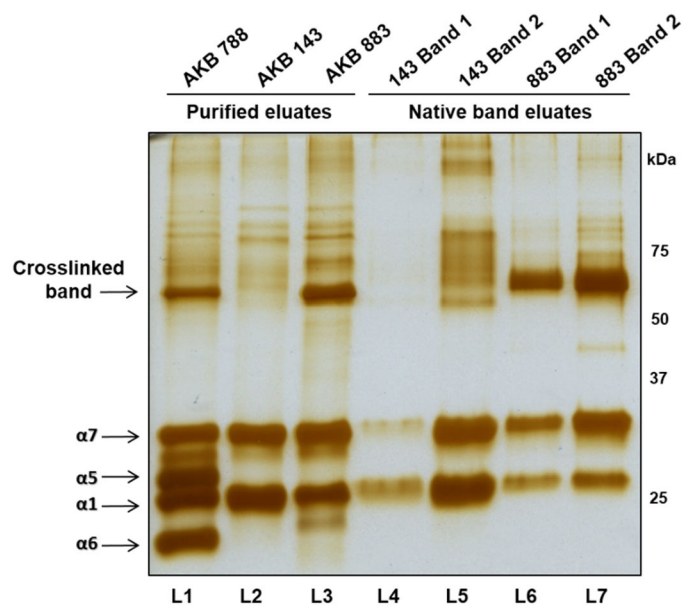


Figure 25. Crosslinking analysis of high molecular weight complexes (HMWCs) formed when  $\alpha 7$  and  $\alpha 1$  are co-expressed. (a) HMWCs of AKB143 and AKB883 shown in Figure R24 were excised from the gel and the proteins were eluted under non-reducing conditions. These eluates were electrophoresed on 12% denaturing gel alongside non-reduced eluates of AKB143 and AKB883 originally affinity purified by IMAC. The gel was visualized by silver staining. Cross-linked bands are indicated.

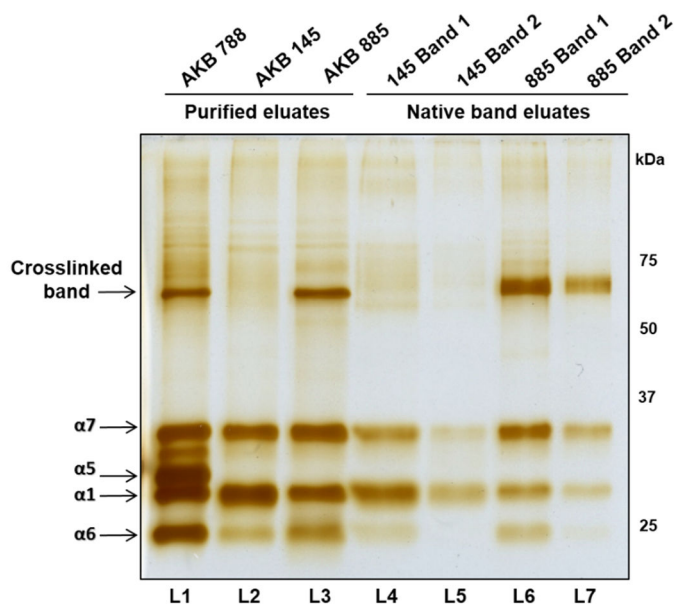


Figure 26. Crosslinking analysis of high molecular weight complexes (HMWCs) formed when  $\alpha 6$ ,  $\alpha 7$  and  $\alpha 1$  are co-expressed. (a) HMWCs of AKB145 and AKB885 shown in Figure R24 were excised from the gel and the proteins were eluted under non-reducing conditions. These eluates were electrophoresed on 12% denaturing gel alongside non-reduced eluates of AKB145 and AKB885 originally affinity purified by IMAC. The gel was visualized by silver staining. Cross-linked bands are indicated.